Aus der Klinik für Anaesthesiologie

Klinikum der Ludwig-Maximilians-Universität München

Direktor: Prof. Dr. med. Bernhard Zwißler

Dissertation

zum Erwerb des Doctor of Philosophy (Ph. D.)

an der Medizinischen Fakultät der

Ludwig-Maximilians-Universität München

MDSC-specific mechanisms of T cell immunoparalysis after Cardiopulmonary Bypass

vorgelegt von

Max Bernhard Hübner

aus

Berlin

2021

Mit Genehmigung der Medizinischen Fakultät der

Ludwig-Maximilians-Universität zu München

First evaluator (1. TAC member): Prof. Dr. Dr. Simone Kreth

Second evaluator (2. TAC member): Prof. Dr. Friedrich-Wilhelm Kreth

Third evaluator: Prof. Dr. Barbara Schraml-Schotta

Fourth evaluator: Priv.-Doz. Dr. Ulrich Grabmaier

Dean: Prof. Dr. med. Thomas Gudermann

Date of the defense:

December 22nd, 2021

Abstract

Cardiopulmonary bypass (CBP) is associated with severe immune dysfunctions. Particularly, a CBP–associated long-lasting immunosuppressive state renders patients prone to a higher risk of postoperative complications, such as persistent bacterial infections. We investigated the mechanisms underlying this phenomenon, and were able to detect a transiently occurring cell population that strongly suppresses T cell function after CBP. This cell population was identified as Myeloid-Derived Suppressor Cells (MDSC) that are assumed to emerge from the myeloid lineage. Currently, however, only scarce data regarding the real origin of MDSCs are available and the mechanisms that mediate their strong immunosuppressive potential are largely elusive.

This thesis aimed at elucidating the origin of MDSC and at characterizing MDSC-mediated mechanisms that account for post-cardiopulmonary bypass immunosuppression. We combined molecular methods, e.g. flow cytometry, real-time PCR and functional T cell assays with a comprehensive gene expression analysis by means of Next-Generation Sequencing (NGS). We could identify L-Arginine depletion caused by Ariginase overexpression and excessive production of Reactive Oxygen Species (ROS) as MDSC-specific mechanisms of postoperative T cell immunosuppression and revealed that supplementation of L-Arginine or ROS scavengers such as reduced Glutathione (GSH) or N-Acetylcysteine (NAC) hampers T cell immunosuppression. Moreover, we could show that MDSC display a gene expression profile strongly differing from granulocytic cells suggesting that these cells indeed represent a separate cell entity. Taken together, this study identified two MDSC-specific mechanisms that contribute to T cell immunoparalysis observed after CPB and proposes therapeutic strategies to overcome postoperative immunosuppression.

Table of contents

Abstract **1**

Table of contents **3**

1. Introduction **5**

1.1 CPB: Principle, components, construction 5

1.2 Cardiac surgery and CPB - Impact on the immune system- Severe Inflammatory Response Syndrome (SIRS) and concomitant immunoparalysis 6

1.3 MDSC as novel key players during post-CPB immunosuppression 7

1.4 MDSC: history and origin 11

2. Materials and methods **13**

2.1 Patient recruitment 13

2.2 Sampling of blood 13

2.3 Serum asservation and PBMC isolation 13

2.4 Cell counting and viability assessment 14

2.5 Cell culture and media 14

2.6 Microbead Separation 15

2.7 Arginase Activity Assay 15

2.8 CFSE dilution assay 16

2.9 Enzyme-Linked Immunosorbent Assay (ELISA) 17

2.10 RNA extraction and cDNA synthesis 17

2.11 Real-time quantitative reverse transcription polymerase chain reaction (qRT-PCR) 17

2.12 Protein lysis and SDS-PAGE 18

2.13 Flow Cytometry and intracellular staining 19

2.14 Liquid Chromatography-Tandem Mass Spectrometry and Mass Spectrometry Measurements 19

2.15 Next-Generation Sequencing (NGS) 20

2.16 NGS Bioinformatics 20

2.16.1 Downstream analysis 20

2.16.2 Reads mapping to the reference genome 21

2.16.3 Quantification of gene expression levels 21

2.16.4 Differential expression analysis (For DESeq2 with biological replicates) 21

2.16.5 Clustering 21

2.16.6 GO and KEGG enrichment analysis of differentially expressed genes 21

2.16.7 Protein-Protein Interaction (PPI) analysis of differentially expressed genes 22
2.17 Measurement of intracellular GSH concentrations 22
2.18 Statistical Analysis 22
3. Results 23
3.1 MDSC-mediated T cell immunosuppression after CPB - role of L-Arginine metabolism 23
3.2 L-Arginine levels after CPB - impact on T cell immune function.....26
3.3 L-Arginine supplementation ameliorates MDSC-induced immune cell suppression. ...26
3.4 Detailed characterization of post CPB-MDSC.....29
3.5 Differential gene expression in Granulocytes, Low-density Granulocytes (LDG) and MDSC.....29
3.6 Specific gene expression profile in post-CPB MDSC – pathways 35
3.7 Comparison of T2 MDSC and T2 granulocytes - focus on T cell immunosuppressive genes.....36
4. Discussion.....42
5. References.....46
6. Acknowledgments 50
7. Appendix.....51

1. Introduction

The use of extracorporeal circulation and oxygenation devices, later on referred to as Cardiopulmonary Bypass (CPB), started 60 years ago.[1] This dramatically expanded the portfolio of cardiac surgery as it enabled surgeons to perform more complex interventions in complete cardioplegia. Since the 1980s, surgical interventions that do not necessarily require CPB (so-called off-pump surgery), for example off-pump coronary artery bypass grafting (CABG) or endoluminal valve replacements have been developed. Despite the continuous development of novel methods for off-pump surgery,[2] CPB is still essential for a large number of cardiac interventions that require complete cardioplegia. Thus, CPB still represents an indispensable and continuously developing technique in cardiac surgery.

1.1 CPB: Principle, components, construction

In general, CPB replaces the function of the heart and the lung during cardioplegia: aortic cross-clamping separates the systemic circulation from the cardiac output. To maintain circulation and provide oxygen to organ tissues, blood is collected from cavoatrial or bicaval cannulation sites and pumped into extracorporeal silicone tubing by a roller or centrifugal pump unit that generates a non-pulsatile, continuous flow. Next, the blood is introduced into a heat exchanger that allows for temperature control of the blood. If desired, this setup allows surgical procedures in cardioprotective hypothermia. Subsequently, the blood passes through an oxygenator. Finally, the oxygenated blood is reintroduced into the patient via an arterial cannulation site that is mainly located in the distal part of the ascending aorta (Fig. 1).[3]

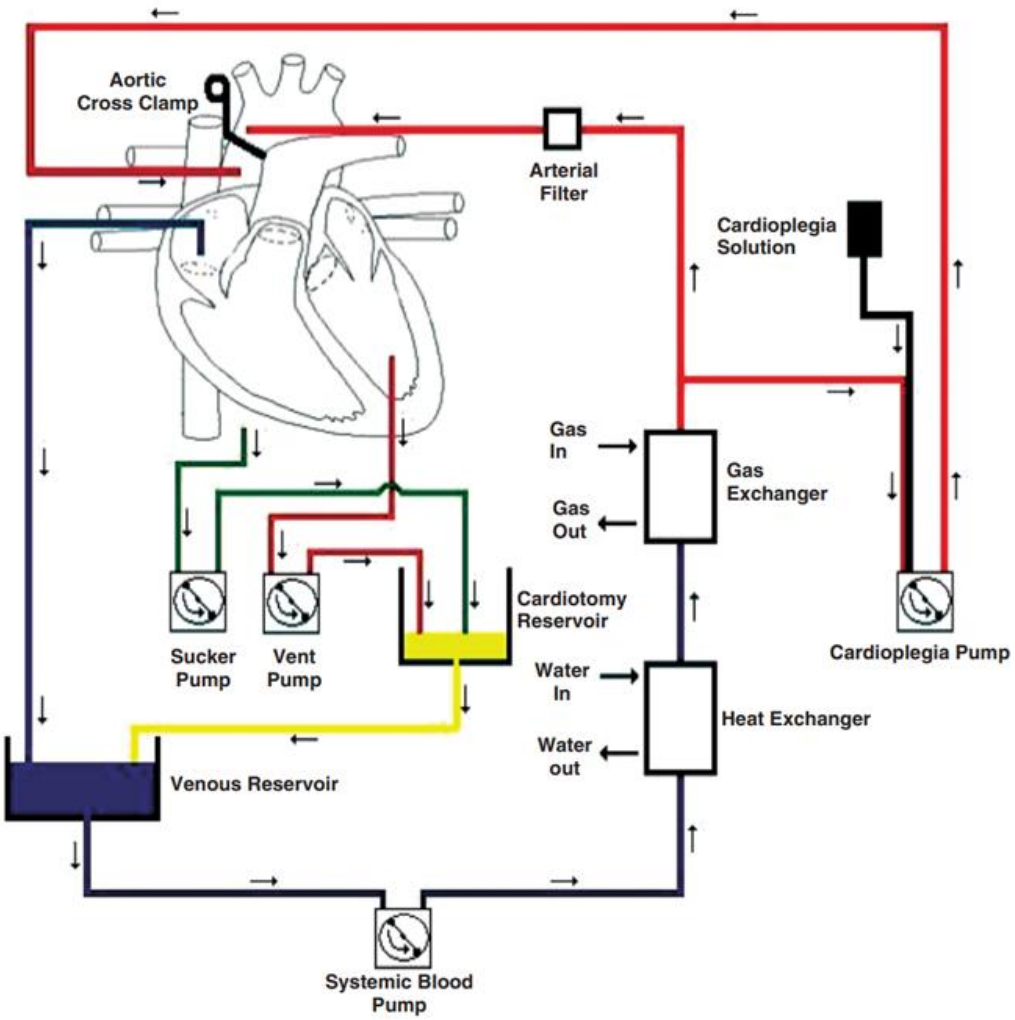

Figure 1. Principle and components of CPB. Picture obtained from: Machin, D. & Allsager, C. Principles of cardiopulmonary bypass. Contin Educ Anaesth Crit Care Pain 6, 176–181 (2006).

1.2 Cardiac surgery and CPB - Impact on the immune system- Severe Inflammatory Response Syndrome (SIRS) and concomitant immunoparalysis

During cardiac surgery, the immune system is strongly affected by several factors: surgical injury, cardiac manipulation, CPB tubing and ischemia/reperfusion phenomena. All these factors induce a strong inflammatory immune response known as Severe Inflammatory Response Syndrome (SIRS) mainly mounted by innate immune cells.

Simultaneously, longer-lasting anti-inflammatory reactions are initiated[4–6] (Fig. 2), which frequently lead to an immunosuppressive state putting patients at risk for secondary

complications such as wound healing disorders, secondary infections, prolonged stay in the ICU or even death.[7–11] The molecular mechanisms underlying this strong immunosuppression, however, are less clear and to date, no effective therapy exists.

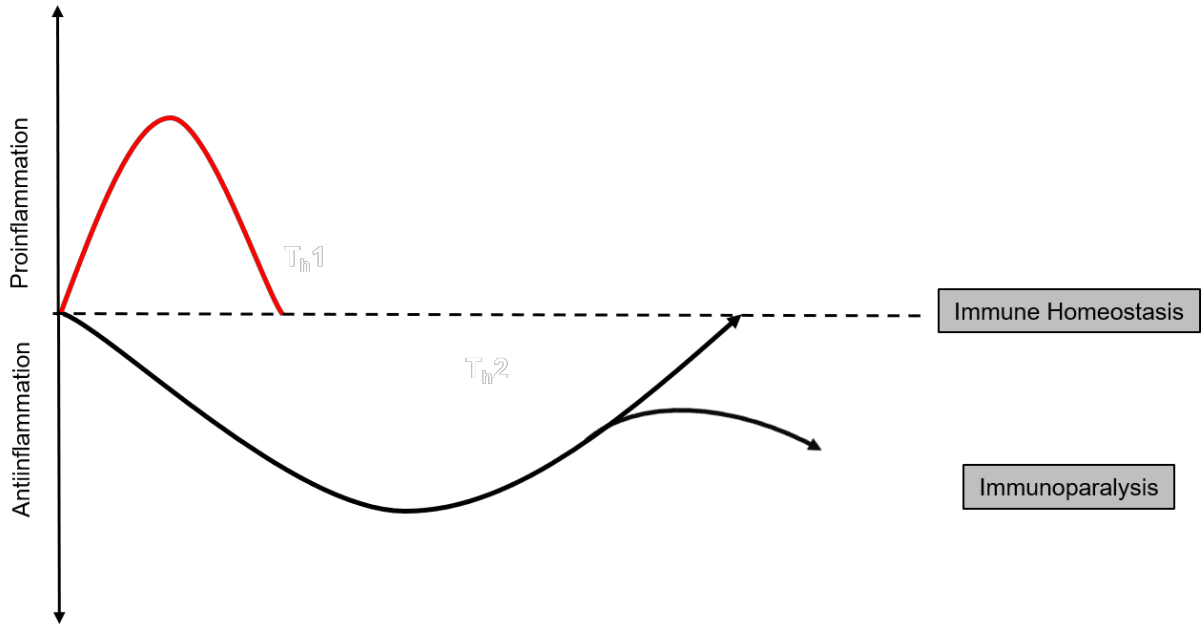

Figure 2. Schematic overview of immune responses during cardiac surgery and CPB. Surgical stimulus and CPB mount a quick, short-lasting pro-inflammatory immune response (red graph) and, concomitantly, longer-lasting anti-inflammatory reactions (black graph). This immunoparalytic state increases the risk for a „second hit" such as infections or wound healing disorders. Graph modified from Hotchkiss, R. S., Monneret, G. & Payen, D. Immunosuppression in sepsis: a novel understanding of the disorder and a new therapeutic approach. Lancet Infect. Dis. 13, 260–268 (2013).

1.3 MDSC as novel key players during post-CPB immunosuppression

Recently, by analysing T cell effector functions such as IFNɣ secretion, T cell specific proliferation or -cell lysis capacity, we could prove that cells of the adaptive immune system are indeed considerably hampered after CPB (Fig. 3).[12]

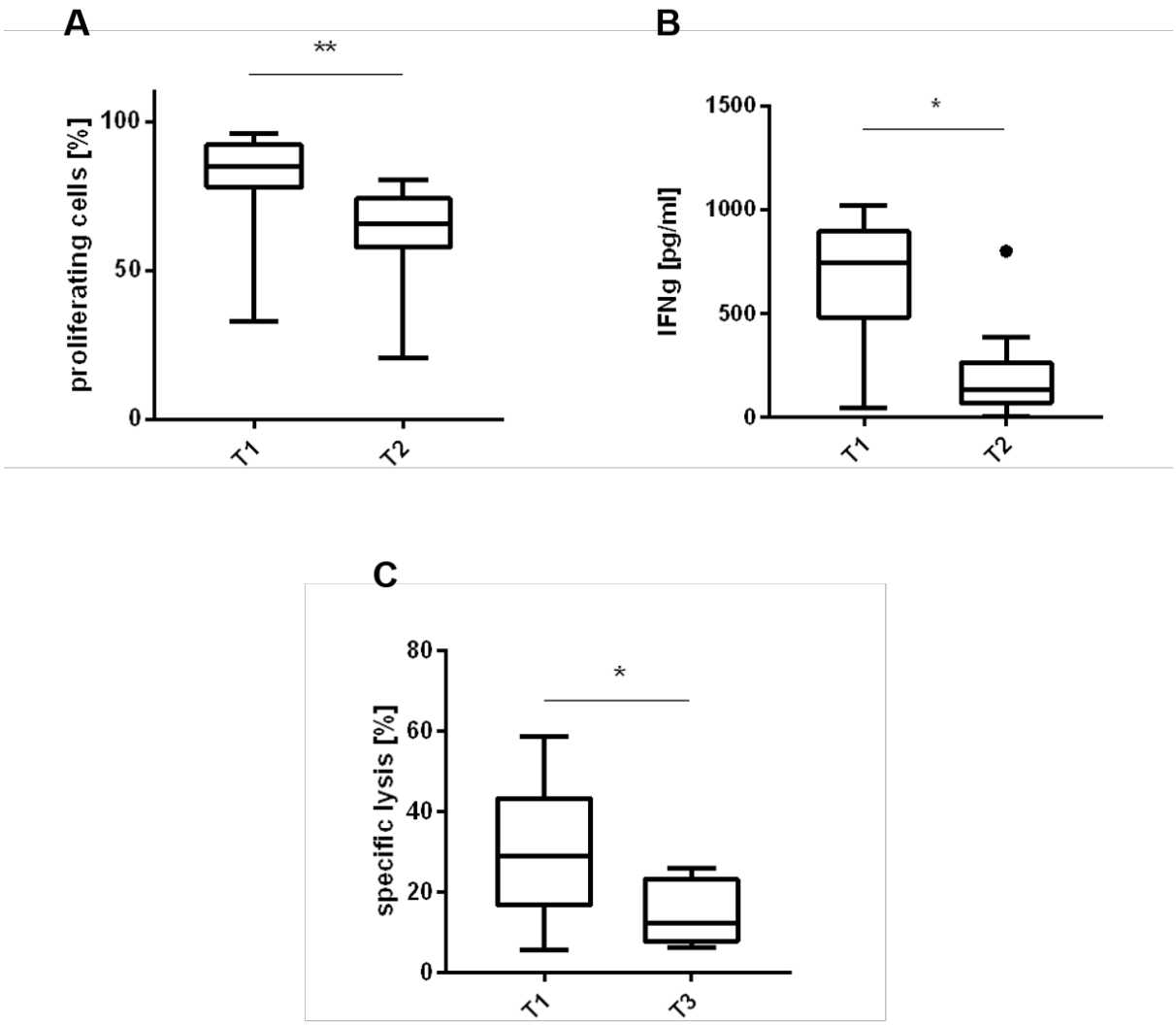

Figure 3. CPB induces immunosuppression. Effector functions before CPB (T1), directly after CPB (T2) and on the first postoperative day (T3). **A)** Proliferation rates measured by carboxyfluorescein succinimidyl ester dilution assay after T cell specific stimulation with anti-CD3/CD28 microbeads and incubation for 6 days (n=10, $p<0.01$). **B)** Interferon (IFN)-γ cytokine secretion measured by ELISA after in-vitro stimulation with anti CD3/CD28 microbeads for 5 days (n=10, p=0.043). **C)** $CD8^+$-specific lysis of Calcein-labeled K562 target cells after incubation for 4 hours (n=6, p=0.024).

Moreover, we discovered a novel mechanism contributing to the immunoparalytic phenotype observed after CPB: CPB triggers a transient accumulation of Myeloid-Derived Suppressor Cells (MDSC) since the novel population detected after CPB fulfilled the morphologic criteria for MDSC ($CD14^+$, HLA-DR^-, $CD11b^+$, $CD15^+$)[13] as analyzed by flow cytometry and May-Grünwald-Giemsa staining (Fig. 4 and Table 1).[12]

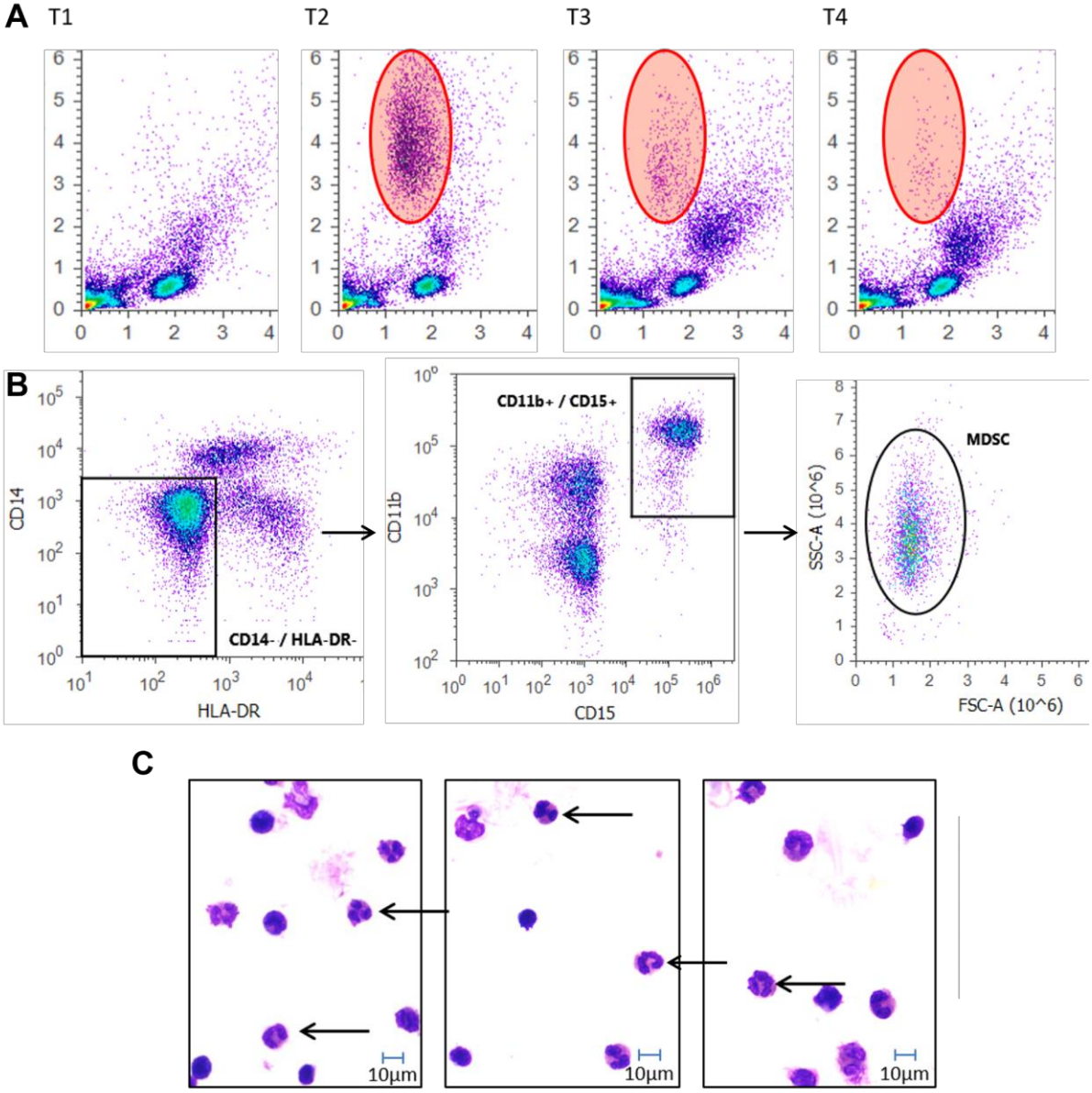

Figure 4. CPB induces a transiently occurring cell population fulfilling the morphologic criteria for MDSC. **A)** Flow cytometry of unstained PBMC detected a transient cell population occurring directly after CPB (T2), gradually diminishing on the first postoperative day (T3) until ICU discharge (T4). **B)** Gating strategy of the flow cytometry-based immunophentopying of PBMC after CPB. Novel cell population expresses markers recommended to identify MDSC ($CD14^+$, $HLA\text{-}DR^-$, $CD15^+$, $CD11b^+$). Cells were analyzed after doublet exclusion. C) May-Grünwald-Giemsa staining of the transient cell population reveals a granulocytic-myeloid morphology.

	T2	T3	T4
MDSC [%]	15.3 ± 1.5	7 ± 1.2	9.2 ± 1.7
Minimum	0.27	1.1	1.6
Maximum	50.1	59.5	32.1
25th	4.6	3.1	3.1
75th	20.9	7.6	14.9

Table 1. Absolute Numbers of cells expressing MDSC markers, time points T2 – T4. Depicted are mean, minimum, maximum, 25th and 75th percentile (n=66).

Current recommendations for unambiguous identification of MDSC, however, demand functional analyses in order to corroborate the immunosuppressive potential of the analysed cell population. To assess whether the transient cell population indeed suppresses T cell function, we selectively depleted these cells by CD15 microbead separation. Subsequent flow cytometric analysis showed that cells fulfilling MDSC criteria were not detectable in the CD15-negative fraction and that a large body of the CD15-positive fraction expresses MDSC markers (Fig. 5).[12]

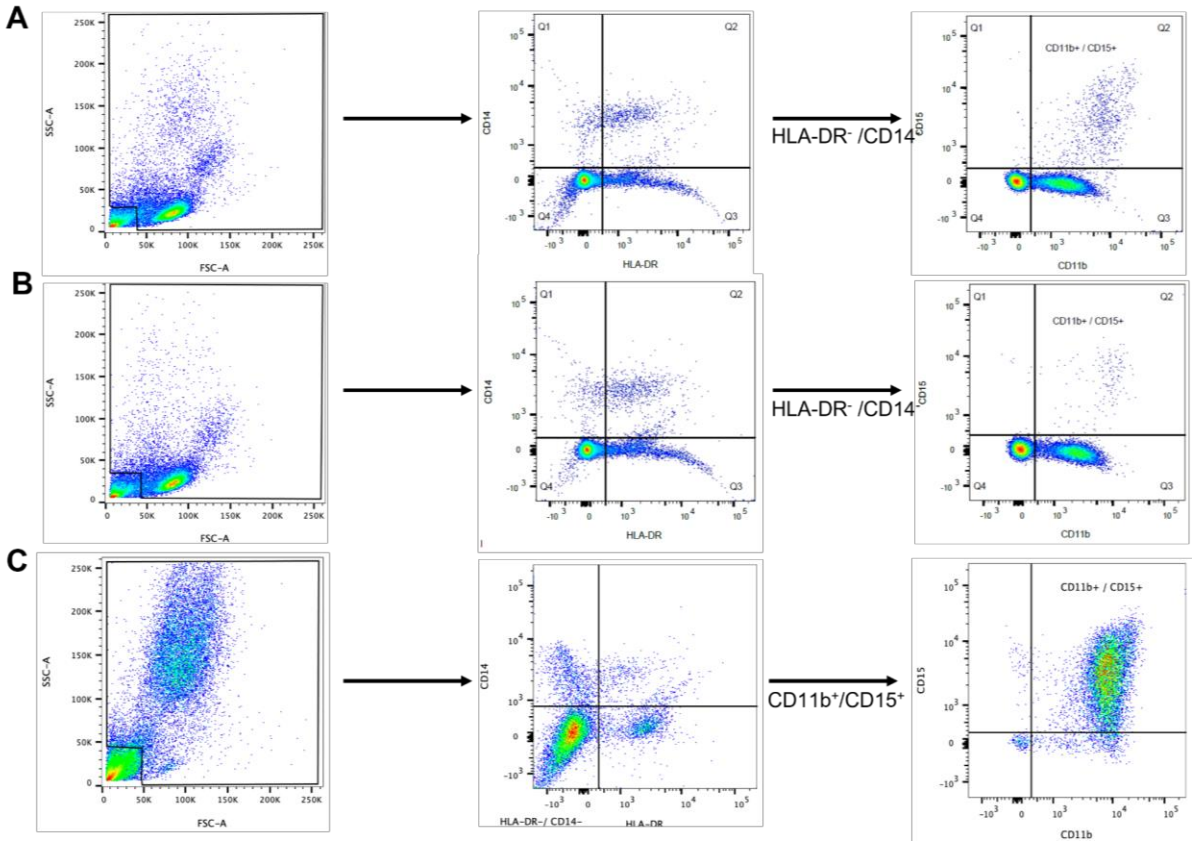

Figure 5. CD15 microbead separation of T2 PBMC depletes novel cell population expressing MDSC markers. **A)** PBMC obtained from time point T2 before and **B)** after depletion of CD15$^+$ cells. **C)** Expression of MDSC-markers in the positive fraction after CD15 microbead separation.

Finally, we analyzed effector functions in the presence (+ CD15) or absence (-CD15) of CD15$^+$ cells and could prove that effector functions are significantly impaired in the presence of CD15$^+$ cells, ultimately corroborating that the novel cell population detected after CPB indeed represents MDSC. (Fig. 6)[12]

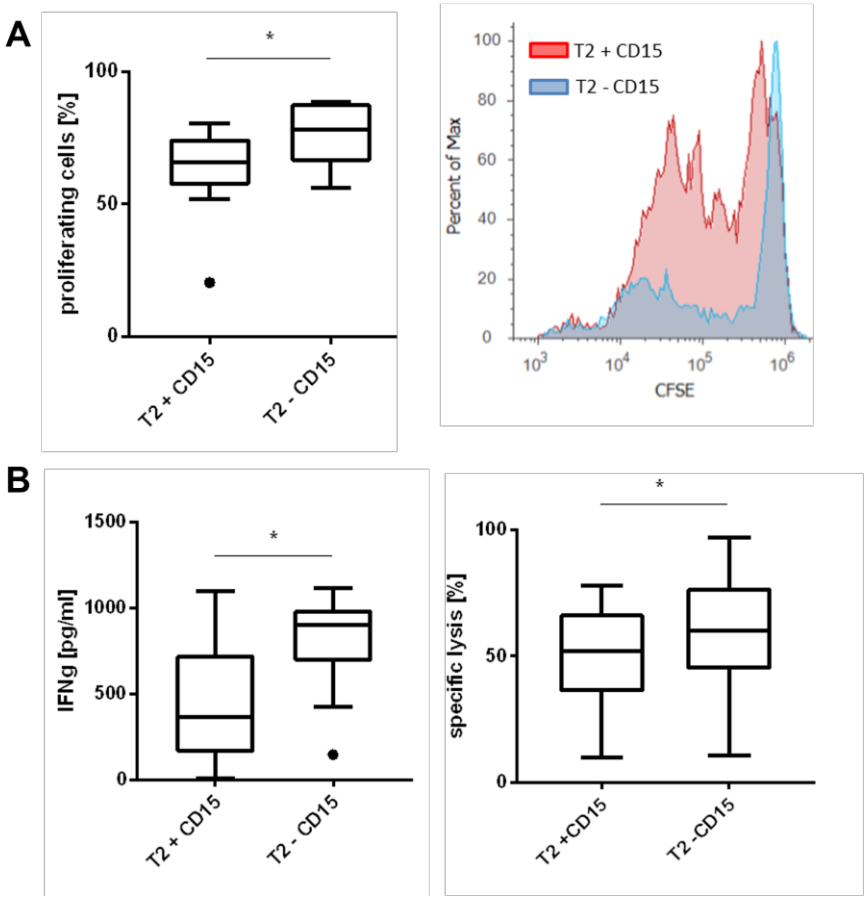

Figure 6. CPB-induced MDSC suppress T cell function. Functional analyses were conducted using T2 PBMC containing $CD15^+$ cells (+CD15) or after depletion of $CD15^+$ by microbead separation (-CD15). **A)** left: proliferation rates as measured by CFSE dilution assay. Right: one representative histogram of independently conducted CFSE dilution assays of T2 PBMC, PBMC were activated by antiCD3/CD28 beads after CFSE labeling and incubated für 5 days. **B)** left: IFNɣ levels in cell culture supernatants as measured by ELISA after in-vitro stimulation with anti-CD3/CD28 beads for 5 days. Right: specific lysis of Calcein-labeled K562 target cells.
(n=10, $p<0.05$ for all experiments).

1.4 MDSC: history and origin

MDSC were first described in the late 1990s as cells with granulocytic morphology and either monocytic ($CD14^+$) or hematopoietic progenitor ($CD34^+$) markers,[14,15] co-purifying with Peripheral Blood Mononuclear Cells (PBMC) after Ficoll density gradient centrifugation and displaying T cell suppressive properties.[16]

However, MDSC are normally not detected in healthy individuals except in neonates or during pregnancy.[17,18] Prior to our study, MDSC were rather identified during chronic inflammatory disorders only such as cancer[16,19,20] or autoimmune diseases like Lupus Erythematodes[21,22] and Rheumatoid Arthritis.[23,24] Although only very low amounts of MDSC

can be detected in the patients' peripheral blood during chronic inflammation, their strong immunosuppressive properties dramatically impair T cell immunocompetence.[16,25] Thus, despite displaying monocyte and neutrophil markers and -morphology, their functional and biochemical properties differ significantly from monocytes or neutrophils.[17,18]

The exact origin of MDSC is currently unknown; one assumption is that MDSC simply represent peripherally activated granulocytes as stimulation of granulocytes with N-Formylmethionine-leucyl-phenylalanine (fMLP) resulted in co-purification of granulocytes in the mononuclear layer after Ficoll gradient centrifugation, showing a surface activation marker profile similar to MDSC.[26]

In contrast, other studies support the notion that MDSC rather represent immature, pathologically activated myeloid cells[27] being unable to differentiate into mature myeloid cells and prematurely egress from the bone marrow into the peripheral blood.[19]

MDSC were previously detected in chronic inflammatory disorders only. However, they here appeared in a rather unpredictable time course and very low cell numbers. Thus, a model to reproducibly investigate the molecular mechanisms of MDSC was previously unavailable and the mechanisms that account for their strong immunosuppressive properties largely remained elusive. Now, in view of the reproducible appearance of MDSC after CPB, we are capable to investigate the mechanisms of MDSC-mediated immunosuppression in a more detailed manner.

Hence, this thesis aims at

1. characterizing the gene expression profile of MDSC and comparing it to other cells of the myeloid lineage
2. identifying MDSC-specific mechanisms that account for T cell immunoparalysis after CPB
3. evaluating potential treatment strategies that dampen post-CPB immunosuppression.

2. Materials and methods

2.1 Patient recruitment

This study was approved by the local ethics committee of the Ludwig-Maximilians-University Munich (approval number: 17–241). Written informed consent from patients electively scheduled for cardiac surgery with planned use of the CPB was obtained before study inclusion. The following characteristics resulted in exclusion from the study: age <18 years, emergency surgery, pregnancy, known malignancies, acute inflammatory processes prior to surgery, previous organ transplantation, immune system dysfunction or immunosuppression, steroid treatment and decline of study participation. Anesthesia was performed following an internal protocol: no premedication was applied; general anesthesia was induced with sufentanil 0.5-1 µg/kg, thiopental 2.5-5 mg/kg and rocuronium 0.5-1 mg/kg, and maintained by continuous administration of 0.7-1.2 µg/kg/h sufentanil and 1.5-2 Vol% sevoflurane. During surgery, muscle relaxation was maintained by intravenous, fractionized application of Rocuronium. After intuvation, all patients experienced pressure-controlled ventilation, applying tidal volumnes of approximately 6-8ml/kg weight.

2.2 Sampling of blood

For each time point, blood was drawn from the arterial catheter routinely inserted prior to the surgical procedure. 18ml of blood was drawn in tubes containing lithium heparin (Sarstedt, Germany). For serum asservation, 9ml of blood was drawn into a serum tube. Time points for blood draw were after induction of anesthesia before (T1) and after(T2) the application of the CPB circuit, on the first postoperative day (T3) and upon discharge from the ICU (T4). Heparinized blood was processed immediately after collection.

2.3 Serum asservation and PBMC isolation

In 9ml serum tubes, the serum was placed on the bench and the blood was allowed to clot for approximately 30 minutes at room temperature. To remove cells, the serum tube was centrifuged at 3000 rpm for 10 minutes afterwards. The resulting supernatant was aliquoted in smaller amounts and immediately stored at -80°C (Heraeus, Germany). The heparinized portion of the blood was used for PBMC isolation using Ficoll density gradient centrifugation. Thus, the blood was carefully layered on the top of a cell separation medium previously

aliquoted in 14ml plastic tubes (Sarstedt, Germany). For PBMC isolation the density of the cell separation medium (Histopaque®1077, Sigma-Aldrich, USA) was 1,077g/ml and contained Ficoll as well as sodium diatrizoate. After layering, the plastic tubes were centrifuged for 17 minutes at 400 x g. During this procedure, no centrifuge brake was applied, and centrifuge acceleration was performed carefully (4/10). After centrifuging, the PBMC-containing "buffy coat" was extracted from the cell separation preparation, introduced into new 14ml plastic tubes and underwent two washing steps with Phosphate-Buffered Saline Solution (PBS, Apotheke Innenstadt, University Hospital LMU Munich) at 400xg and 4°C for 10 minutes with medium acceleration (5/10) and brake (6/10).

2.4 Cell counting and viability assessment

For cell counting, cells were first resuspended in 1ml PBS after the final washing step. Next, 20µl of the cell suspension was diluted in 480µl PBS, introduced in a cell counting sample cup. Cell number and -viability was assessed on a Vi-Cell XR (Beckman Coulter, USA) according to manufacturer's instructions with 50 pictures per sample taken automatically. Viability above 95% was a prerequisite for proceeding to further experimentation.

2.5 Cell culture and media

PBMC were maintained in Roswell Park Memorial Institute (RPMI)- medium supplemented with 10% FCS (Biochrom, Germany), 1% L-Glutamine (Gibco, USA) and 1% HEPES (Gibco, USA) in a humidified atmosphere at 37°C and 5% CO_2 using a cell culture incubator (Binder, Germany). Cell density was 1 Mio PBMC/ml. T cell specific activation of PBMC was performed by adding microbeads conjugated with antiCD3/CD28 antibodies (Thermo Fisher, USA) at a density of 12.5 µl beads per $0.75x10^6$ PBMC. L-Arginine supplementation utilized either a custom-formulated RPMI medium containing 150µM of L-Arginine or normal RPMI medium. However, both formulations included 10% FCS, 1% L-Glutamine and 1% HEPES. For experiments involving ROS scavenging, the above mentioned normal RPMI formulation was either supplemented with 5mM N-Acetyl-Cysteine (NAC) or 5mM reduced Glutathione (GSH, both Merck, Germany).

2.6 Microbead Separation

For separation of MDSC, PBMC were incubated with magnetic beads (microbeads) conjugated with a CD15 antibody (Miltenyi Biotec, Germany, cat. no. 130-046-601). After centrifugation, the cell pellet was resuspended in 80µl buffer A (PBS, 0.5% bovine serum albumin (BSA), and 2 mM EDTA, pH 7.2 per 10^7 cells. Next, 20µl CD15 microbeads were added, the suspension was mixed and incubated for 15 minutes in the refrigerator at 2-8°C. Thereafter, cells were washed by adding 2ml of buffer A per 10^7 cells and centrifuged at 300xg and 4°C for 10 minutes. The cell pellet was resuspended in 500µl buffer A and the cell suspension was introduced in the AutoMACS™ Pro Separator (Miltenyi Biotec, Germany) using the program "Possel". After separation, the negative cell fraction was discarded. The positive cell fraction was centrifuged, resuspended in 500µl PBS and counted on a Vi-Cell XR cell analyzer. An appropriate amount of cells was immediately lysed in RNA (Qiagen, Germany) or protein lysis buffer supplemented with phosphatase inhibitors (both (Cell Signalling Technology, USA).

For separation of granulocytes, StraightFrom™ Whole Blood CD15 MicroBeads (Miltenyi Biotec, Germany, cat. no. 130-091-058) were used according to the manufacturer's instructions. Briefly, 2ml of heparinized whole blood were passed through a 30µm nylon mesh (Miltenyi Biotec, Germany). Next, 50µl of the microbead suspension were added, the suspension was mixed and incubated for 15 minutes in the refrigerator at 2-8°C. After incubation, 10ml buffer A was added, the cell suspension was washed twice and finally resuspended in buffer A to a total volume of 2ml. The cell suspension was placed in the AutoMACS™ Pro Separator and the program "Posselwb/Rinse" was applied to isolate CD15 positive granulocytes. The positive fraction was centrifuged, resuspended in 500µl PBS and counted on a Vi-Cell XR cell analyzer (Beckman Coulter, USA). An appropriate amount of cells was immediately lysed in RNA (Qiagen, Germany) or protein lysis buffer. (Cell Signalling Technology, USA)

2.7 Arginase Activity Assay

Arginase activity was analysed using the Arginase Activity Assay Kit (Sigma Aldrich, USA) according to manufacturer's instructions. Briefly, urea contamination was first depleted from serum samples b transferring 100 µL of serum to filters for ultracentrifugation (cut-off of 10 kDa, Merck, Germany). After addition of 400µl nuclease-free water, centrifugation was

carried out at 4°C and 14.000 rpm for 30 minutes. After discarding the fluid that passed through the membrane, 500µl of nuclease-free water was pipetted on the filters and they were centrifuged again. Thereafter, 40 µl of the remaining supernatant were transferred to a 96 well plate and 10µl of the 5x Substrate Buffer that contained L-Arginine and Manganese were added. Controls containing water, serum sample without addition of the Urea reagent and Urea standards were carried along the throughout the whole assay After incubation for 2 hours in an incubator at 37°C, 200µl of the Urea reagent, composed of 100 µl Reagent A and 100 µl Reagent B supplied with the kit in order to stop the Arginase reaction and the plate was incubated at room temperature for 60 minutes. Finally, absorbance was measured at 430nm and Arginase activity was calculated according to the following formula:

$$\text{Activity} = \frac{(A_{430})_{sample} - (A_{430})_{blank}}{(A_{430})_{standard} - (A_{430})_{water}} \times \frac{(1\ \text{mM} \times 50 \times 10^3)}{(V \times T)}$$

T = Reaction time in minutes
V = sample volume (µL) added to well (1–40 µL)
1 mM = concentration of Urea Standard
50 = reaction volume (µL)
10^3= mM to µM conversion factor

2.8 CFSE dilution assay

A total number of 750,000 PBMC/well were labeled with CFSE (Biolegend, USA). This was performed in 1ml PBS at a final CFSE concentration of 1µM. Labelling incubation was conducted for 20 minutes un a humidified cell culture incubator (37°C, 5%CO2). CFSE labelling was terminated and by addition of 5ml RPMI medium containing with 10% FCS. Cells were stimulated as previously stated in section 2.5 and maintained in RPMI medium with 10% FCS, 1% L-Glutamine and 1% HEPES. After stimulation, 30 IU Interleukin-2 (Miltenyi Biotec, Germany) was added to the media. Incubation was maintained for 5 days without disturbance or medium change. Then anti-CD3/CD28 beads were removed magnetically during cell harvest. After two washing steps with 1%BSA PBS, CFSE dilution was assessed by flow cytometry. By using the Attune Acoustic Focusing Cytometer software, the amount of $CFSE^{dim}$ cells was analyzed (Thermo Fisher, USA).

2.9 Enzyme-Linked Immunosorbent Assay (ELISA)

Cell supernatant obtained from the incubation experiments performed in section 2.8 as was immediately stored at –80°C after harvesting. ELISA analysis was conducted by transferring 100 µL of cell culture supernatant to the 96-well ELISA assay plate (LEGEND MAX Human Interferon γ [IFNγ] ELISA Kit, Cat. No. 430107; Biolegend, USA) and processed according to the manufacturer's instructions. IFN γ was directly proportional to the optical density of the wells, assessed on a microplate reader (Molecular Devices, Germany) at a wavelength of 450nm.

2.10 RNA extraction and cDNA synthesis

RNA extraction (1×10^6 cells) was performed using the RNEasy kit (Qiagen, Germany) with a subsequent DNA digestion step (DNAse treatment). RNA concentration was measured using a Nano Drop 2000 spectrophotometer (Thermo Fisher). Equal amounts of RNA were reversely transcribed into complementary DNA (cDNA) using Oligo dT Primers, Random Hexamers (Qiagen), deoxynucleotide triphosphates (Roche, Switzerland), RNAse OUT, and Superscript III Reverse Transcriptase (both Thermo Fisher, USA). Briefly, Oligo-dT Primers, Random Hexamers and dNTP were added to the RNA samples and incubated in a thermal cycler (Mastercycler, Eppendorf, Germany) at 65°C für 5 minutes. Thereafter, samples were cooled down for 1 minute on ice. Subsequently, First Strand Buffer, DTT, Superscript Reverse Transcriptase (all Thermo Fisher) and RNAse OUT (Ambion, USA) were added to the respective RNA samples. Reverse Transcription was performed on a thermal cycler (Eppendorf) and includes incubation for 5 minutes at 25°C, followed by 45 minutes at 50°C and a final incubation period of 15 minutes at 70°C. Thereafter, samples were immediately stored at -20°C.

2.11 Real-time quantitative reverse transcription polymerase chain reaction (qRT-PCR)

qRT-PCR analyses were performed on a LightCycler 480 (Roche, Switzerland) in duplicate using Universal Probe Library (UPL) probes (Roche) and specifically designed primers (Metabion, Germany). Succinate dehydrogenase subunit A (SDHA) and TATA Box Binding Protein (TBP) were used as reference genes in all experiments. Primer sequences are given in Table 2. All assays were designed intron spanning. RT-PCR conditions comprising

initial denaturation for 10 minutes (95 °C), and 50 cycles of 95 °C for 10 seconds, 60 °C for 30 seconds and 72 °C for 1 second. Quantification cycle (Cq) values and relative mRNA expression was calculated using the LightCycler® Quantification Software (Roche).

Name	Primer Sequence	UPL Probe #
TBP	Forward 5`-GAACATCATGGATCAGAACAACA-3` Reverse 5`-ATAGGGATTCCGGGAGTCAT-3`	87
SDHA	Forward 5`-GAGGCAGGGTTTAATACAGCA-3` Reverse 5`-CCAGTTGTCCTCCTCCATGT-3`	132
ARG1	Forward 5` CCTCCTGAAGGAGCTAAAAGGAA 3` Reverse 5` CCTTGGCAGATATACAGGGAGT 3`	2
MPO	Forward 5`-AAGCTCCGGGATGGTGAT-3` Reverse 5`-GATCCGGGGCAATGAGAT--3`	81
NOX2	Forward 5`-GGCTTCCTCAGCTACAACATCT-3` Reverse 5`-GTGCACAGCAAAGTGATTGG-3`	20
SOD1	Forward 5`-TCCATGTTCATGAGTTTGGAGAT-3` Reverse 5`-CCCACCGTGTTTTCTGGATA-3`	40
CD3zeta	Forward 5`-GGCACAGTTGCCGATTACA-3` Reverse 5`-ATTCCATCCAGCAGGTAGCA-3`	40

Table 2. Primer sequences for qRT-PCR.

2.12 Protein lysis and SDS-PAGE

For the preparation of protein lysates, $1x10^6$ cells were lysed in a cell lysis buffer supplemented with protease/phosphatase inhibitors (Cell Signaling Technologies, USA). After incubation for 5 minutes on ice, cells were sonified and centrifuged at 13,200 rpm at 4°C. The supernatant was collected, and protein concentration was assessed by BCA assay (Thermo Fisher) according to the manufacturer's instructions. Equal amounts (20µg) of protein were electrophoretically separated on SDS-polyacrylamide gels and blotted on PVDF membranes using a Trans Blot® Turbo™. Arginase1 expression was detected using a rabbit monoclonal antibody (clone D4E3M, Cat. No. 9819, Cell Signaling). ß-Actin (Clone 13E5, Cat. No. 4970, Cell Signaling) served as an endogenous loading control. Horseradish-labeled goat anti-mouse or goat anti-rabbit antibodies (Cell Signaling) were used to detect immunoreactive bands after incubation of the membrane with Signal Fire ECL substrate (Cell Signaling). Chemiluminescence was detected using the Aequoria dark box and the Orca-ER detection system (Hamamatsu, Japan).

2.13 Flow Cytometry and intracellular staining

Freshly isolated PBMC or MDSC ($0.25x10^6$) were washed twice and resuspended in 100µl PBS containing 1% Bovine Serum Albumin (BSA, Roth, Germany) (FACS buffer). Prior to staining, nonspecific binding was blocked by adding 5µl Human TruStain FcX™ Fc receptor blocking solution (Biolegend, USA, cat. no. 422302) and incubation for 10 minutes at room temperature. Thereafter, cells were incubated with fluorophore-conjugated antibodies for 20 minutes on ice. and washed twice and resuspended in 1ml FACS Buffer afterwards.

For intracellular staining, PBMC or MDSC ($0.25x10^6$) stained with the desired surface fluorophore-conjugated antibodies, washed twice and resuspended in 100µl FACS buffer. Subsequently, cells were fixed and permeabilized using the FoxP3/Transcription Factor Staining Buffer Set (Thermo Fisher, USA) according to the manufacturer's instructions. Briefly, 100µl of IC fixation buffer was added to the cell suspension, mixed by vortexing and incubated for 45 minutes at room temperature in the dark. Next, the cell suspension was washed twice by adding 2ml of permeabilization buffer and centrifugation at 500xg for 5 minutes. Thereafter, the pellet was resuspended in 100µl permeabilization buffer and subsequently stained with 2.5µl of the desired fluorophore-conjugated antibody, either Arginase1 (PE, Biolegend, cat no. 369705, clone no. 14D2C43) or CD3zeta (FITC, cat no. 644103, clone no. 6B10.2). Cells were washed twice and resuspended in 1ml FACS Buffer. Flow cytometric data was collected by selective gating on lymphocytes or MDSC, measuring 100.000 events per tube. Unstained and isotype controls were used to determine autofluorescence and nonspecific antibody binding. Multicolor Compensation was carried out using UltraComp eBeads (Thermo Fisher). Analysis of flow cytometry data was performed with FlowJo Software Version 10 (FlowJo LLC, USA).

2.14 Liquid Chromatography-Tandem Mass Spectrometry and Mass Spectrometry Measurements

Quantification of L-Arginine serum concentrations were performed in collaboration with the laboratory of Prof. Dr. Schwedhelm, Institute of Clinical Pharmacology and Toxicology, University Medical Center Hamburg-Eppendorf, Hamburg, Germany as described previously.[28] In brief, 25µL-aliquots of serum were diluted with 100 µL 2H7-L-Arginine dissolved in methanol. Proteins were precipitated and residues were derivatized to their butylester derivatives. Reconstituted samples were injected into the 1,200 L Triple Quadrupole

MassSpectrometry/Mass Spectrometry system (Agilent Technologies, Germany). Analytes were separated on a Polaris C18-Ether column (Agilent Technologies; 50 × 2.0 mm) using an elution gradient of the two mobile phases: A) 1 mL/L formic acid in water and B) acetonitrile-methanol (50/50, volume/volume) containing 1 mL/L formic acid at a flow rate of 0.3 mL/min. The ion transitions m/z 231 greater than 70 and m/z 238 greater than 77 were recorded over time for quantification of L-Arginine and deuterium-L-Arginine, respectively. The analytical range of the method was validated for 0–250 µmol/L L-Arginine, and intra- and inter assay coefficients of variation were below 15%.

2.15 Next-Generation Sequencing (NGS)

NGS was performed by Novogene (Great Britain) according to the company's specific protocol. In brief, sequencing libraries were generated using the QuantSeq 3' mRNA-Seq Library Prep Kit FWD for Illumina (Lexogen GmbH, Austria). The PCR Add-on Kit for Illumina (Lexogen GmbH, Austria) to determine the optimal number of amplification cycles. Amplification was conducted according to the manufacturer's protocol. Quality and quantity of sequencing libraries were determined using the Quanti-iT PicoGreen dsDNA Assay Kit (Invitrogen, USA) and the Bioanalyzer High Sensitivity DNA Analysis Kit (Agilent Technologies, Inc., USA). Sequencing of libraries was performed on an Illumina HiSeq4000 sequencing machine (Illumina, Inc., USA). Individually barcoded libraries were pooled and distributed across lanes of the same flow-cell aiming for approximately ten million paired-end reads per sample.

2.16 NGS Bioinformatics

Data analysis was conducted by Novogene (Great Britain) according to the following methods:

2.16.1 Downstream analysis

Downstream analysis was performed using a combination of programs including STAR, HTseq, Cufflink and our wrapped scripts. Alignments were parsed using Tophat program and differential expressions were determined through DESeq2/edgeR. Gene Ontology (GO) and Kyoto Encyclopedia Of Genes And Genomes (KEGG) enrichment were implemented by the ClusterProfiler.

2.16.2 Reads mapping to the reference genome

Reference genome and gene model annotation files were downloaded from the genome website browser (NCBI/UCSC/Ensembl) directly. Indexes of the reference genome was built using STAR and paired-end clean reads were aligned to the reference genome using STAR (v2.5).

2.16.3 Quantification of gene expression levels

HTSeq v0.6.1 was used to count the read numbers mapped of each gene. Next, Fragments per kilobase per million mapped reads (FPKM) of each gene was calculated based on gene length and mapped read counts. [29].

2.16.4 Differential expression analysis (For DESeq2 with biological replicates)

Differential expression analysis between two conditions/groups (two biological replicates per condition) was performed using the DESeq2 R package (2_1.6.3).. The resulting P-values were adjusted using the Benjamini and Hochberg's approach for controlling the False Discovery Rate(FDR). Genes with an adjusted P-value <0.05 found by DESeq2 were assigned as differentially expressed. Prior to differential gene expression analysis, for each sequenced library, the read counts were adjusted by the edgeR program package through one scaling normalized factor. Differential expression analysis of two conditions was performed using the edgeR R package (3.16.5). The P-values were adjusted using the Benjamini & Hochberg method. Corrected P-value of 0.05 and absolute fold change of 1 were set as the threshold for significantly differential expression. The Venn diagrams were prepared using the function Venn Diagram in R based on the gene list for different group.

2.16.5 Clustering

To identify the correlation between differences in gene expression, samples were clustered using expression level FPKM to see the correlation using hierarchical clustering distance method with the function of heatmap, SOM (Self-organization mapping) and means using silhouette coefficient to adapt the optimal classification with default parameter in R.

2.16.6 GO and KEGG enrichment analysis of differentially expressed genes

GO enrichment analysis of differentially expressed genes was implemented by the clusterProfiler R package, in which gene length bias was corrected. GO terms with corrected P-value less than 0.05 were considered significantly enriched by differential expressed genes.

statistical enrichment of differential expression genes in KEGG pathways was assessed by the clusterProfiler R package.

2.16.7 Protein-Protein Interaction (PPI) analysis of differentially expressed genes

PPI analysis of differentially expressed genes was performed using the target genes list of the publicly available STRING database.[30]

Differentially expressed gene annotation TFCat, a curated catalog of mouse and human transcription factors (TF) based on a reliable core collection of annotations obtained by expert review of the scientific literature and Cosmic, a database designed to store and display somatic mutation information and related details which contains information relating to human cancers were used to annotate the differential expressed gene.

2.17 Measurement of intracellular GSH concentrations

Measurement of intracellular GSH concentrations was performed using the ThiolTracker™ Violet (Glutathione detection reagent, Thermo Fisher, USA) according to manufacturer's instructions. This dye actively reacts with reduced thiols in intact cells. Briefly, 200,000 cells ($CD4^+$ or $CD8^+$ cells obtained by microbead separation (Miltenyi, Germany) were resuspended in 1ml PBS containing 1µl of a 10mM stock solution of ThiolTracker™. The suspension was mixed by pipetting and incubated for 30 minutes at 37°C in the dark. Thereafter, cells were washed once with 1ml PBS, centrifuged for 5 minutes at 400xg and the supernatant was discarded. Cells were resuspended in 200µl PBS and fluorescence was immediately analyzed on a FACSCanto (BD, USA) at an emission of 526nm.

2.18 Statistical Analysis

All data were analyzed using GraphPad prism 7 (GraphPad Software, USA) and tested for normal distribution using the D′Agostino Pearson normality and Shapiro-Wilk tests. For parametric distribution, differences between groups were analyzed by two-tailed paired or unpaired Student t test. For nonparametric distribution, data were analyzed using the Wilcoxon signed rank test. p values less than 0.05 were considered statistically significant (*$p < 0.05$; **$p < 0.01$). If not stated otherwise, values given represent means ± Standard Error Of The Mean (SEM). With the exception of SDS-PAGE and flow cytometric analyses, all measurements were performed at least in duplicate. Each experiment was repeated at least five times.

3. Results

3.1 MDSC-mediated T cell immunosuppression after CPB - role of L-Arginine metabolism

Having established that MDSC are, at least in part, responsible for T cell immunosuppression after CPB,[12] this thesis focuses on clarifying the molecular mechanisms that account for this phenomenon. As MDSC may lead to L-Arginine shortage via increased L-Arginine breakdown and thus strongly hamper T cell function,[31,32] L-Arginine serum levels using Liquid Chromatography-Tandem Mass Spectrometry/Mass Spectrometry (LCMS/MS) were assessed. We detected a significant decrease of serum L-Arginine concentrations on the first postoperative day (T3) (Fig. 7, T1: 81.27 ±3.81 µmol/L; T2: 80.79 ±3.79 µmol/L; T3: 70.96 ±3.35 µmol/L; T4: 92.79 ±5.31; n=33; p<0.05).).

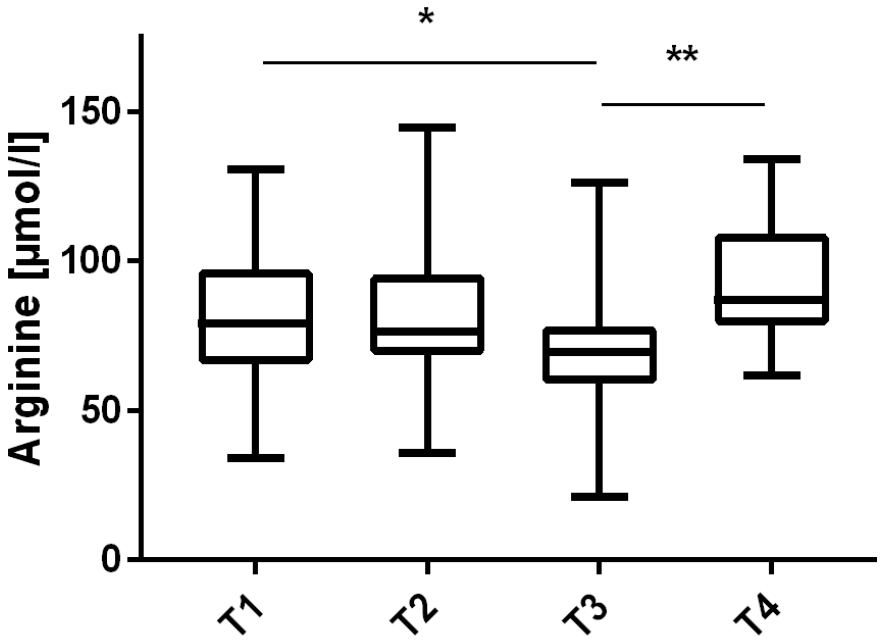

Figure 7. L-Arginine serum levels decrease after CPB. L-Arginine levels in serum obtained from patients before CPB (T1), directly after CPB (T2), on the first postoperative day (T3), and at ICU discharge (T4as measured by liquid chromatography-tandem mass spectrometry) (n = 33; *p < 0.05; **p < 0.01).

Next, to investigate whether L-Arginine levels can be attributed to increased L-Arginine breakdown, Arginase1 mRNA and protein expression before and after CPB were assessed in PBMC. As shown in Figure 8 A, B and C, Arginase1 (ARG1) levels were 40-fold induced after CPB (T2) and remained elevated until ICU discharge (T2: induction 40-fold ± 9; p < 0.01; T3: induction 7.2-fold ± 1.42; p < 0.01; T4: induction 12.4-fold ± 3.7 compared to T1; n = 20; p < 0.01). ARG2, however, was not expressed in PBMC (data not shown). In line with these results, Arginase activity was significantly increased in patient serum after CPB with

peak expression on the first postoperative day (T3) (Fig. 8D; T1: 2.55 ±0.37 U/L; T2: 4.4 ±0.54 U/L; T3: 6.13 ±0.6 U/L; T4: 5.9 ±0.63 U/L; n= 20; $p < 0.01$)

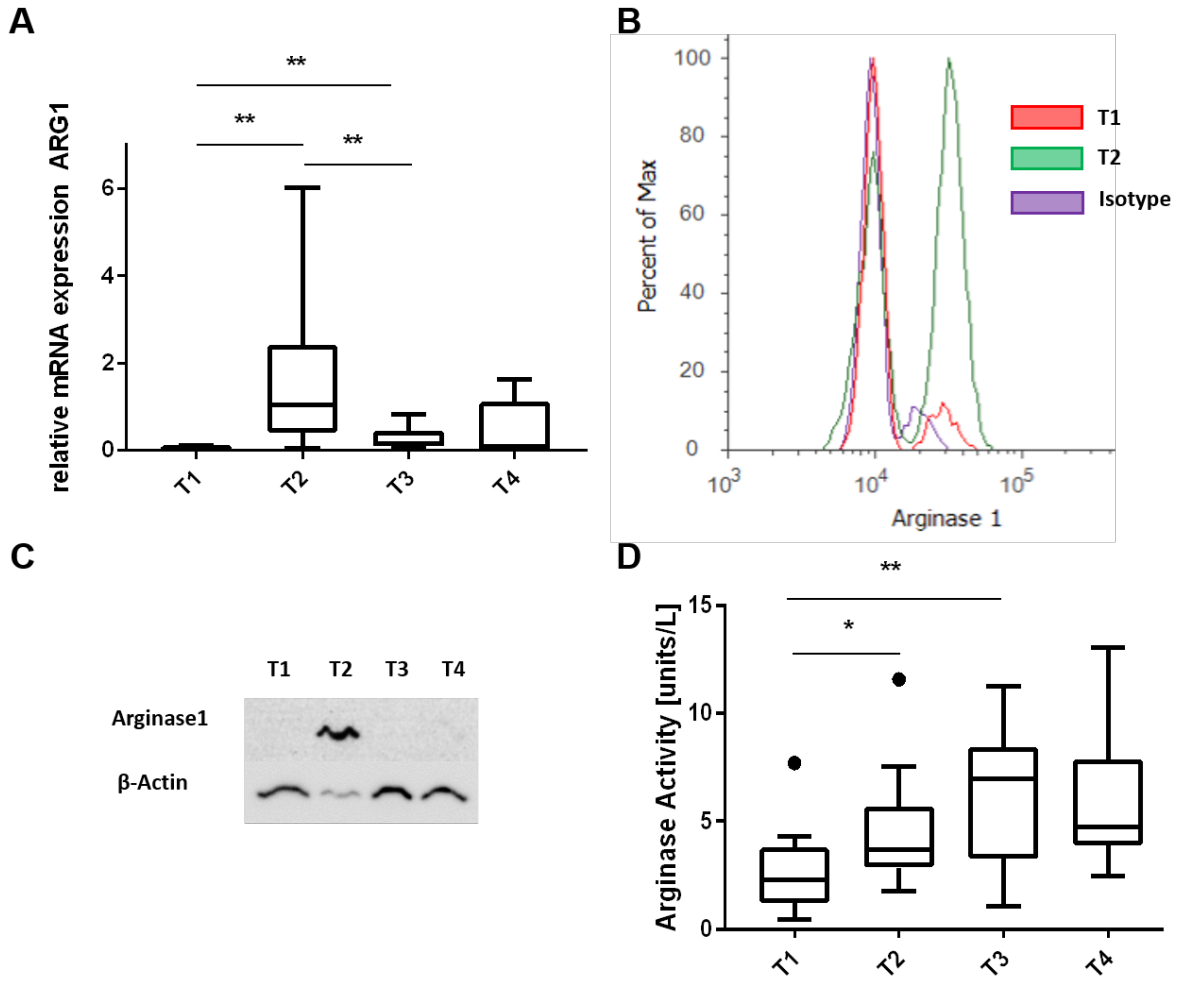

Figure 8. ARG1 expression and Arginase activity are increased after CPB. A) ARG1 mRNA expression in PBMC obtained at time points T1 – T4. (n=20, p<0.01) **B)** Intracellular expression of Arginase1 protein as measured by flow cytometry, time points T1 and T2. One exemplary histogram of five independent experiments is shown. Gating was performed on PBMC after doublet exclusion. **C)** SDS-PAGE of Arginase1 from time points T1 – T4. One representative of three independent experiments is shown. **D)** Arginase activity in patient serum at time points T1-T4 (n=20, p<0.01).

Notably, Arginase serum activity and L-Arginine serum levels after CPB (T2) and on the first postoperative day (T3), respectively, were negatively correlated (Fig. 9; r=-.599, n=13, p=0.031), suggesting that higher Arginase Activity directly after CPB could result in stronger reduction of L-Arginine serum levels on the first postoperative day.

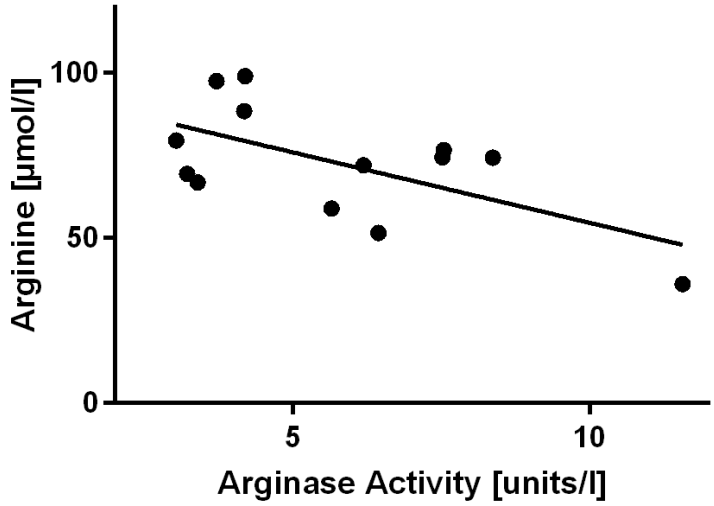

Figure 9. Correlation analysis of T2 Arginase levels and T3 L-Arginine concentrations in patient serum (r=-0.62, n=13, p=0.025).

To provide experimental proof that ARG1 is indeed predominantly expressed in T2 MDSC, PBMC obtained directly after CPB were depleted of MDSC by CD15 magnetobead separation and, subsequently, both fractions were subjected to real-time-PCR, flow cytometry and Western Blot analysis. Compared to T2 PBMC that merely expressed any, ARG1 was abundantly expressed in T2 MDSC (n=6, p=0.03) (Fig. 10). These results suggest that the reduced L-Arginine levels observed are a consequence of increased MDSC-specific L-Arginine breakdown after CPB.

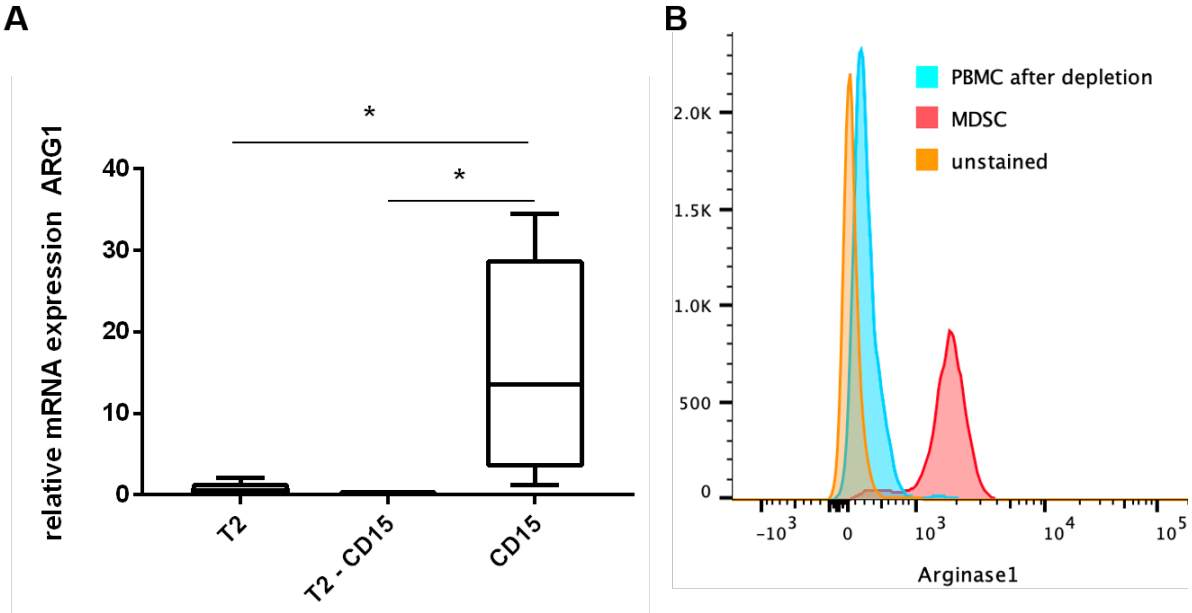

Figure 10. ARG1 is abundantly and specifically expressed in post-CPB MDSC. A) qRT-PCR assessing ARG1 expression in PBMC from time point T2 before (PBMC +CD15), after MDSC depletion (PBMC – CD15), and in the MDSC fraction (CD15) from the same time point, extracted by microbead separation (n = 6; p = 0.03). **B)** Intracellular Arginase 1 expression of T2 PBMC and MDSC as measured by flow cytometry. Blue histogram: PBMC after depletion. Red histogram: MDSC. One representative example of five independent experiments is shown.

3.2 L-Arginine levels after CPB - impact on T cell immune function

L-Arginine levels are of utmost importance for appropriate T cell effector functions: L-Arginine shortage is known to suppress the expression of the CD3 zeta chain (CD3ζ).[33] This central component of the CD3 T cell receptor is located in the inner surface of the cell membrane as a dimer and contains three immunoreceptor tyrosine activation motifs (ITAMs).[34] ITAMs are essential for transduction of the T cell activation signal from the cell surface to the inside as they are required to activate signaling cascades downstream of the T cell receptor. Since six from a total of ten ITAMs of the CD3 receptor are located within the CD3ζ chain,[34] expression of this T cell receptor subunit is crucial to efficiently initiate T cell effector functions. Thus, expression of the CD3ζ chain was analysed, indeed revealing a marked decrease on the first postoperative day (T3) that persisted until ICU discharge (T4) (T3: reduction of 65.5% ±11 compared to T1; n=20, p<0.01) (Fig. 11).

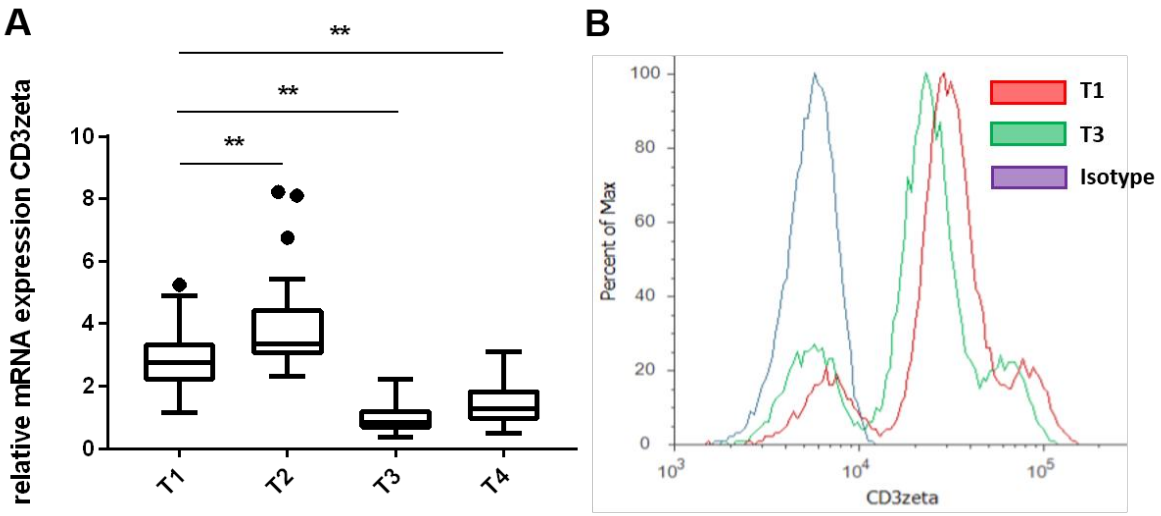

Figure 11. CPB decreases expression of the CD3ζ chain. A) mRNA expression levels of CD3ζ T1-T4 as measured by qRT-PCR (n = 20; p < 0.01). **B)** intracellular flow cytometry of the CD3ζ chain. Gating for CD3**ζ** expression was performed on $CD3^+$ cells after doublet exclusion. One representative example of five independent experiments is shown. Red histogram: before CPB (T1). Green histogram: on the first postoperative day (T3). Purple: isotype control.

3.3 L-Arginine supplementation ameliorates MDSC-induced immune cell suppression.

Postoperative alterations in T cell functions are common after cardiac surgery.[35–37] To clarify whether L-Arginine shortage might, at least in part, account for impaired T cell functions observed after CPB, T2 PBMC including MDSC were stimulated with CD3/CD28-specific antibodies, supplemented with low (150µM) or high (1mM) L-Arginine concentrations and incubated for 5 days. Already during cell harvest, the impact of L-Arginine became

obvious: cell numbers were strongly increased in the high L-Arginine group (low L-Arginine: 2.7 million ±1.7, high L-Arginine: 8.15 million ±0.7; n=5, p=0.016) and, more importantly, also cell viability was clearly improved upon L-Arginine supplementation (low L-Arginine: 62.7% ±4.38, high L-Arginine: 73.32% ±2.1; n=5, p=0.015) (Fig. 12).

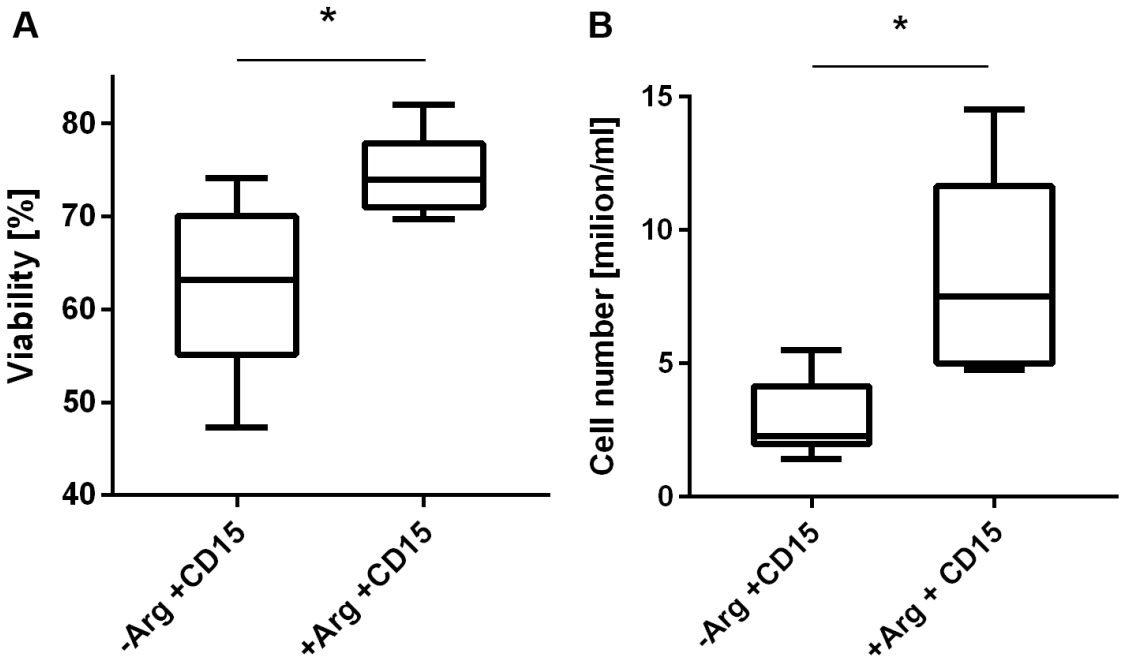

Figure 12. Supplementation of L-Arginine increases cell numbers and improves cell viability. T2 PBMC were stimulated with anti CD3/CD28 microbeads and incubated in RPMI medium containing low (-Arg) and high (+Arg) concentrations of L-Arginine for 5 days. Cell viability (**A**, n=5, p=0.01) and cell numbers (**B**, n=5, p=0.015) were assessed automatically on a Vi-Cell XR.

The effect of L-Arginine supplementation on T cells was corroborated by analyzing T cell effector functions after T cell-specific stimulation with antiCD3/CD28 antibodies: higher L-Arginine doses significantly enhanced the number of proliferating $CD4^+$ (low L-Arginine: 46.74% ±4.43 high L-Arginine: 53.56% ±4.43; n=12, p=0.018) as well as $CD8^+$ T cells (low L-Arginine: 52.84% ±5.43 high L-Arginine: 59.92% ± 4.94; n=12, p<0.01) T cells. Moreover, secretion of the proinflammatory cytokine IFNɣ mainly produced by T cells was strongly improved in the high (1mM) L-Arginine group (low L-Arginine: 432pg/ml ± 54.24; high L-Arginine: 632.8pg/ml ± 63.47; n=11, p=0.023) (Fig. 13). These results suggest that L-Arginine supplementation may ameliorate the immunosuppressive effects of MDSC on T cells and augment T cell survival and effector functions.

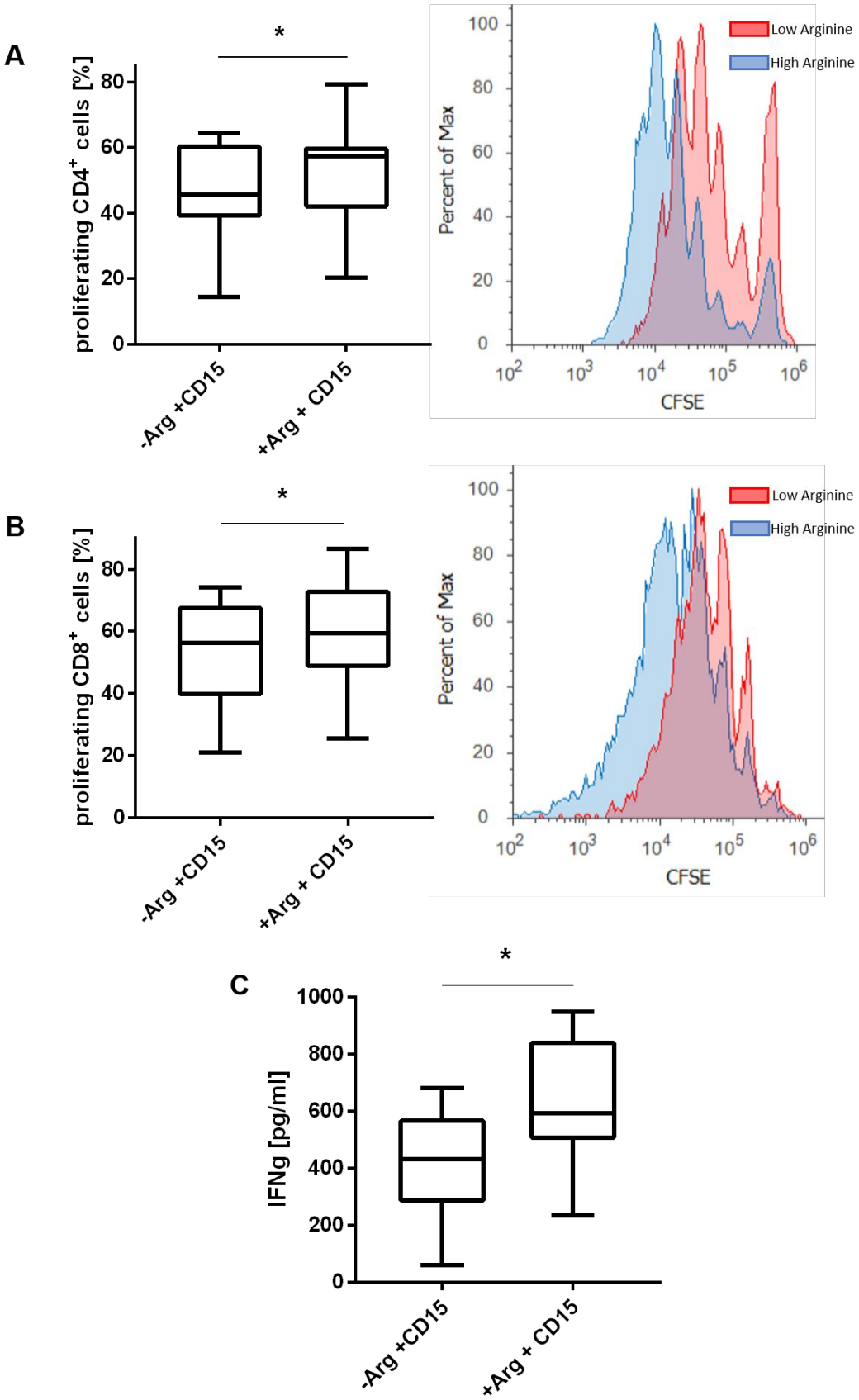

Figure 13. Supplementation of L-Arginine improves effector functions of T cells isolated directly after CPB (T2). After CFSE labeling, T2 PBMC were stimulated with anti CD3/CD28 microbeads and incubated in RPMI medium containing low (-Arg) and high (+Arg) concentrations of L-Arginine for 5 days. Proliferation rates of $CD4^+$ **(A)** and $CD8^+$ **(B)** T cells were analyzed using the CFSE dilution method after doublet exclusion and labelling of CD4 and CD8-positive cells using the respective fluorophore-conjugated antibodies. One representative histogram of 12 independent experiments is shown ($p<0.05$). **C)** IFNγ protein levels in cell culture supernatant as measured by ELISA

3.4 Detailed characterization of post CPB-MDSC

Our results elucidated one MDSC-specific feature that accounts for the immunosuppressive potential of post-CPB MDSC. Earlier studies investigating MDSC in chronic inflammatory diseases like cancer or autoimmune disorders postulated additional mechanisms that, besides L-Arginine depletion, contribute to the suppressive activity of MDSC.[38] Thus, it is more than likely that acute T cell immunosuppression of post-CPB MDSC does not only depend on increased breakdown of L-Arginine.

MDSC were previously detected in very low cell numbers in an unpredictable manner only and no model to induce human MDSC in a reproducible manner existed so far. Consequently, data regarding the MDSC-specific gene expression and their molecular mechanisms that account for the strong immunosuppressive properties are currently lacking. However, by identifying the transient accumulation of MDSC after CPB we recently provided a novel experimental model to investigate the underlying mechanisms of MDSC-mediated immunosuppression in more detail.

Earlier studies suggested that MDSC simply represent degranulated granulocytes and introduced the term "low-density granulocytes (LDG)" to describe these cells with granulocytic morphology that co-purify with PBMC after density gradient centrifugation.[26] However, scarce data suggests that both MDSC and LDG rather represent unique cell populations with distinct immunomodulatory properties.[39] In order to validate that our experimental model indeed detects MDSC, we first performed Next-Generation-Sequencing (NGS) analyses and compared MDSC, LDG and granulocyte gene expression profiles.

3.5 Differential gene expression in Granulocytes, Low-density Granulocytes (LDG) and MDSC

Previous studies reported that LDG were easily inducible by in-vitro stimulation of whole blood with the chemotactic peptide N-Formylmethionine-leucyl-phenylalanine (fMLP).[26] Thus, we first analysed gene expression patterns of fMLP-treated granulocytes and -LDG from the same donors in order to reveal changes specifically occurring during degranulation LDG. Bioinformatics analysis revealed that the rather small number of 585 genes exhibited a differential expression (Fig. 14A and B) between fMLP-treated granulocytes and -LDG (72 up and 513 down). In line with these results, NGS identified only three significantly altered pathways, suggesting that LDG indeed represent a subset of granulocytes (Fig. 14C).

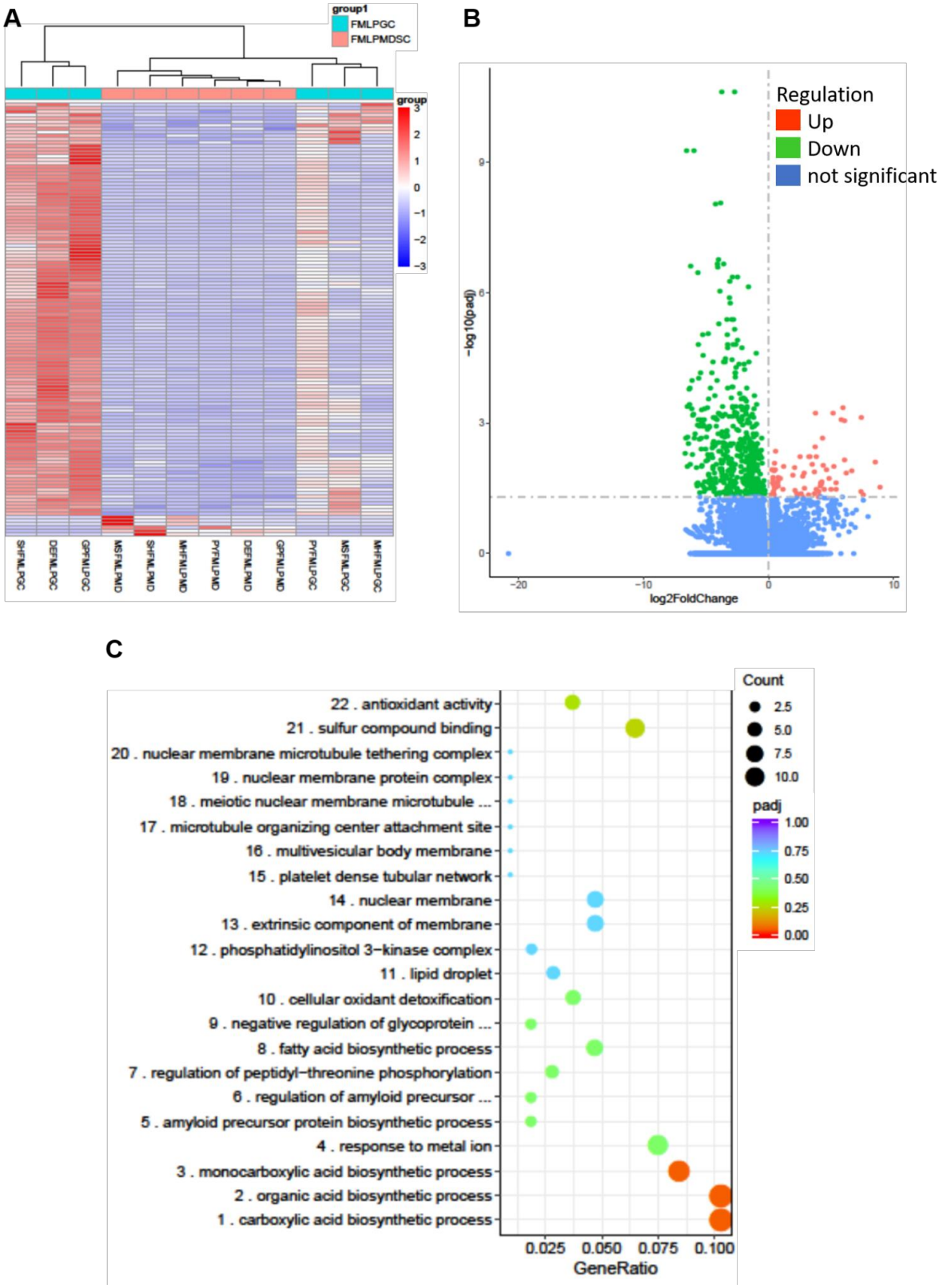

Figure 14. LDG and granulocytes exhibit similar gene expression patterns. Depicted are NGS results from LDG and granulocytes. **A)** Clustered heatmap analysis of differentially regulated genes; downregulation (blue): 513 genes, upregulation (red): 72 genes; n=6, $p<0.05$). **B)** Volcano Plot of significantly up- (red) and downregulated (green) genes. Blue: no significant expression changes between the compared groups. **C)** Gene Ontology (GO) analysis of differentially expressed pathways. Dot size represents the number of regulated genes, dot color represents adjusted p-Value (purple: padj=1; red padj<0.001).

Next, to validate our experimental model and to provide proof that, in contrast to LDG and granulocytes, LDG and post-CPB MDSC indeed significantly differ with respect to their gene expression profiles and pathway expression, we induced LDG in healthy donors by in-vitro fMLP treatment and isolated MDSC from patients after CPB (time point T2). Both cell populations were subjected to NGS and the resulting gene expression profiles were compared. This revealed a dramatically high number of significantly up- (6994) and downregulated (6394) genes (Fig. 15A+B). Moreover, far more than 30 signalling pathways with approximately 50-150 genes per pathway were found to be differentially regulated in T2 MDSC with a p-value below 0.05 (Fig. 15C).

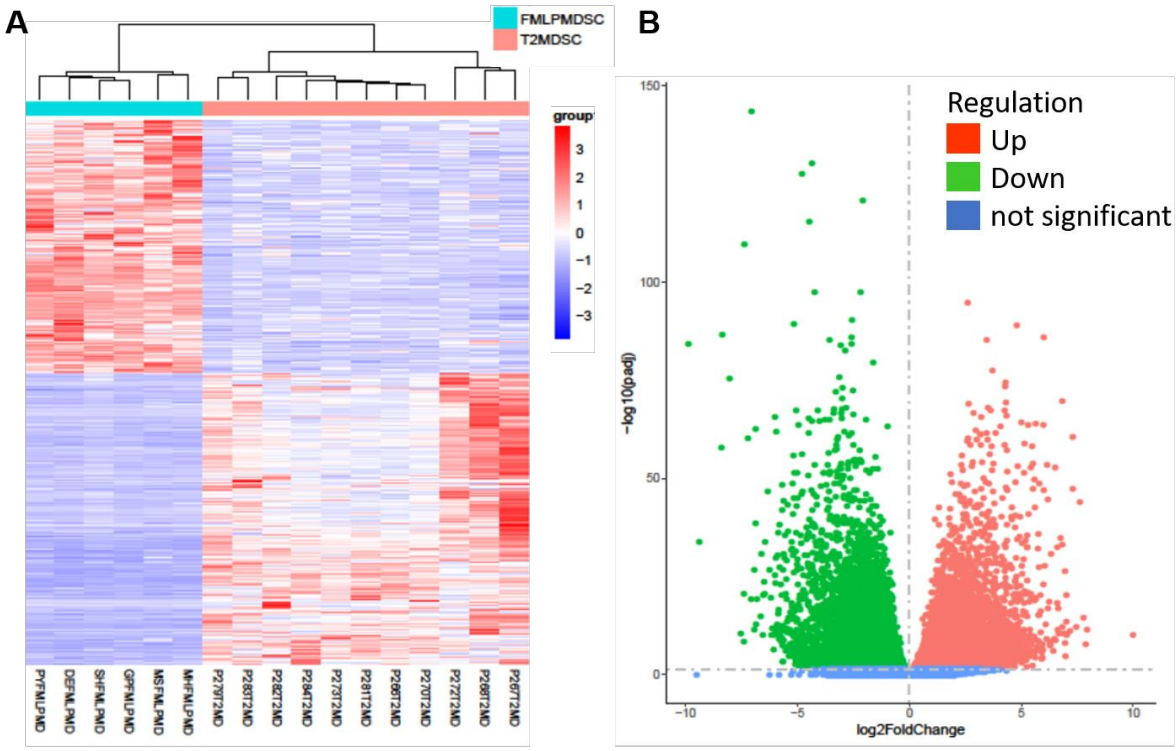

Figure 15. LDG and MDSC display significantly different gene expresison profiles. Comparison of NGS data from LDG (n=6) and T2 MDSC (n=10). **(A)** Clustered heatmap analysis of differentially regulated genes downregulation (blue): 6394 genes, upregulation (red): 6994 genes, ($p<0.05$). **(B)** Volcano Plot of significantly up- (red) and downregulated (green) genes revealing a clear divergence between the two cell entities. Blue: no significant expression changes between the compared groups.

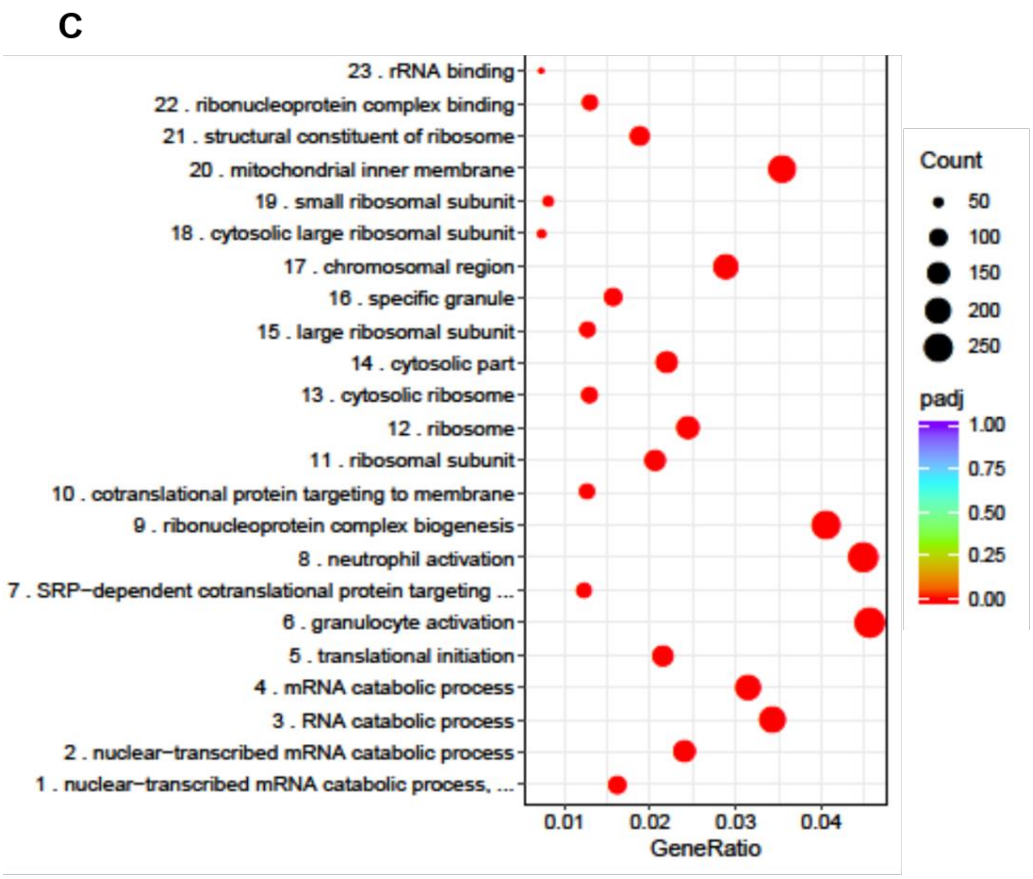

Figure 15. (C) Gene Ontology (GO) analysis of differentially expressed pathways. Dot size represents the number of regulated genes, dot color represents adjusted p-Value (purple: padj=1; red padj<0.001).

Interestingly, pathways involved in RNA processing and protein translation exhibited the strongest and most significant upregulation in MDSC. Moreover, genes involved in granulocyte activation were significantly enriched in T2 MDSC with a rather high gene ratio above 0.04 (Table 3). These results point towards a higher transcriptional activity of MDSC compared to LDG, and provide evidence that post-CPB MDSC do not resemble LDG and indeed represent a unique cell population.

Gene Ontology ID	Description	GeneRatio	p-value	padj	regulated genes
GO:0000184	nuclear-transcribed mRNA catabolic process	0.016181	7.90E-24	4.85E-20	101
GO:0000956	nuclear-transcribed mRNA catabolic process	0.024031	4.83E-23	1.48E-19	150
GO:0006401	RNA catabolic process	0.034284	2.17E-19	4.43E-16	214
GO:0006402	mRNA catabolic process	0.0314	4.29E-19	6.57E-16	196
GO:0006413	translational initiation	0.021467	1.71E-17	2.09E-14	134
GO:0036230	granulocyte activation	0.045658	6.52E-17	6.66E-14	285
GO:0006614	SRP-dependent cotranslational protein targeting to membrane	0.012336	1.61E-16	1.41E-13	77
GO:0042119	neutrophil activation	0.044857	2.32E-16	1.77E-13	280
GO:0022613	ribonucleoprotein complex biogenesis	0.040532	2.61E-16	1.78E-13	253
GO:0006613	cotranslational protein targeting to membrane	0.012656	3.34E-16	2.05E-13	79
GO:0042254	ribosome biogenesis	0.027555	1.10E-15	6.14E-13	172
GO:0034470	ncRNA processing	0.033963	3.48E-15	1.76E-12	212
GO:0002283	neutrophil activation involved in immune response	0.043576	3.73E-15	1.76E-12	272
GO:0002446	neutrophil-mediated immunity	0.044377	4.33E-15	1.89E-12	277
GO:0043312	neutrophil degranulation	0.043255	5.70E-15	2.33E-12	270

Table 3. Differentially expressed processes and pathways in LDG and T2 MDSC according to Gene Ontology (GO) analysis. Gene ratio represents the number of regulated genes divided by the total number of pathway-related genes.

To ultimately provide proof that T2 granulocytes and T2 MDSC strongly differ with respect to their gene expression profiles, we again performed NGS data and analysed the resulting gene expression profiles. This revealed an enormous number of differentially regulated genes (total: 14178 genes, up: 6073 genes, down: 8114 genes, Fig. 16).

So far, these results revealed that T2 MDSC display significantly altered gene expression profiles when compared to T2 granulocytes or LDG. These results clearly revealed that T2 MDSC indeed represent an individual cell population and do not resemble LDG.

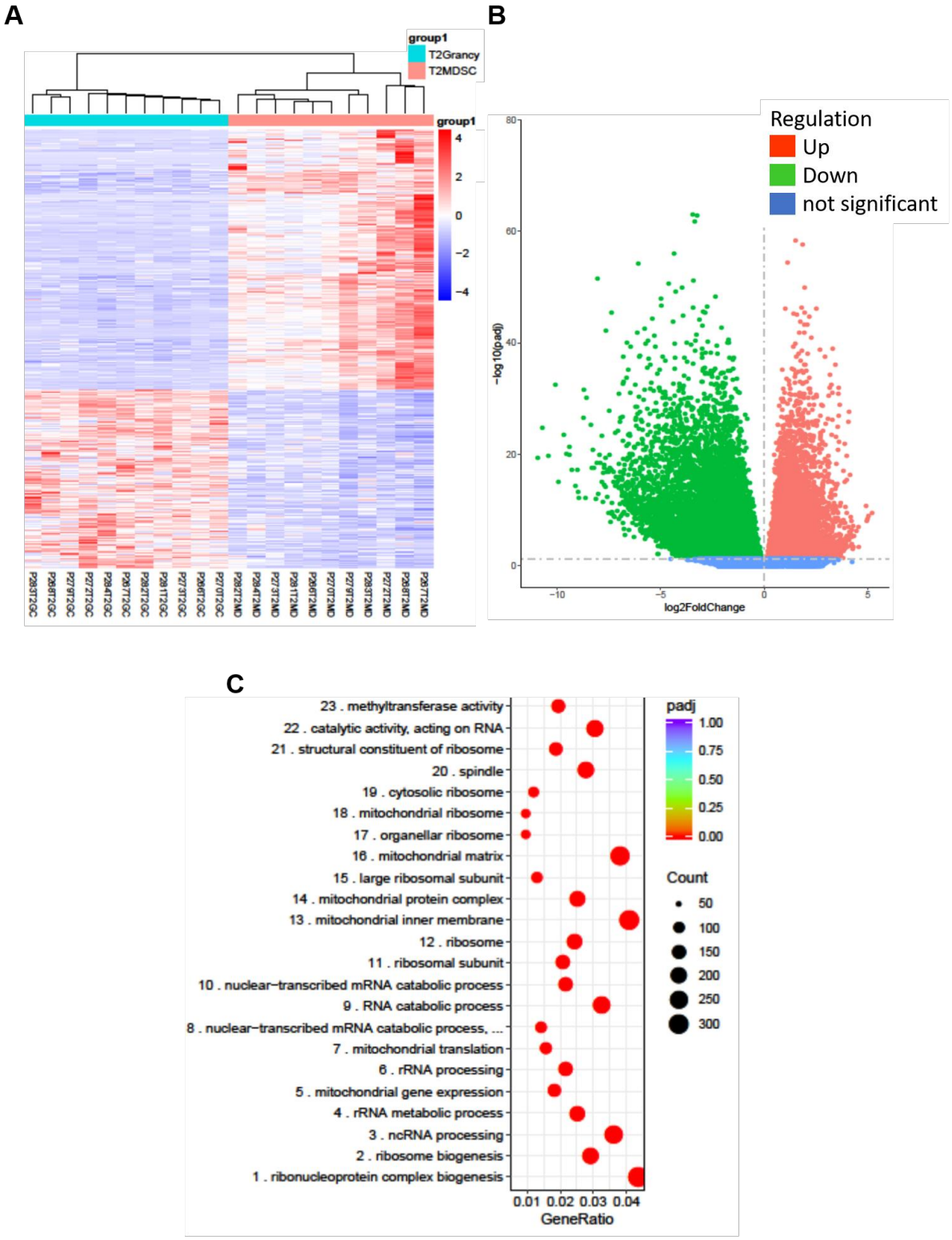

Figure 16. T2 Granulocytes and T2 MDSC strongly differ in their gene expression profiles. NGS data from T2 granulocstes and post-CPB MDSC. **(A)** Clustered heatmap analysis of differentially regulated genes; downregulation (blue): 8114 genes, upregulation (red): 6073 genes; n=11). **(B)** Volcano Plot of significantly up- (red) and downregulated (green) genes. Blue: no significant expression changes between the compared groups. **(C)** Gene Ontology (GO) analysis of differentially expressed pathways. Dot size represents the number of regulated genes, dot color represents adjusted p-Value (purple: padj=1; red padj<0.001).

3.6 Specific gene expression profile in post-CPB MDSC – pathways

Having shown that T2 MDSC indeed strongly differ from mature cell populations of the myeloid lineage such as granulocytes and LDG, NGS data were next analysed in more detail to extract specific genes and pathways that are strongly expressed in MDSC. In line with the results obtained by comparing NGS data of LDG and MDSC, Gene Ontology (GO) search revealed that a disproportionately high number of genes strongly expressed in MDSC were involved in the regulation of transcriptional and translational activity. Specifically, pathways regulating ribosomal biogenesis, mitochondrial gene expression or RNA processing showed a disproportionate number of significantly overexpressed genes, suggesting that MDSC represent a cell entity with high transcriptional activity (Table 4).

Gene Ontology ID	Description	GeneRatio	p-value	padj	regulated genes
GO:0022613	ribonucleoprotein complex biogenesis	0.043448	5.82E-31	3.58E-27	311
GO:0042254	ribosome biogenesis	0.029198	2.03E-27	6.25E-24	209
GO:0034470	ncRNA processing	0.036044	4.39E-27	9.00E-24	258
GO:0016072	rRNA metabolic process	0.025147	1.86E-23	2.52E-20	180
GO:0140053	mitochondrial gene expression	0.018301	2.05E-23	2.52E-20	131
GO:0006364	rRNA processing	0.021654	5.19E-22	5.32E-19	155
GO:0032543	mitochondrial translation	0.015647	9.02E-21	7.93E-18	112
GO:0000184	nuclear-transcribed mRNA catabolic process	0.01425	1.37E-19	1.06E-16	102
GO:0006401	RNA catabolic process	0.032551	3.57E-19	2.44E-16	233
GO:0000956	nuclear-transcribed mRNA catabolic process	0.021654	4.99E-19	3.07E-16	155
GO:0006605	protein targeting	0.03786	5.59E-19	3.12E-16	271
GO:0006614	SRP-dependent cotranslational protein targeting to membrane	0.011735	1.65E-18	8.46E-16	84
GO:0006402	mRNA catabolic process	0.029338	1.71E-17	8.09E-15	210
GO:0006613	cotranslational protein targeting to membrane	0.012015	2.74E-17	1.20E-14	86
GO:0044772	mitotic cell cycle phase transition	0.04261	3.59E-16	1.47E-13	305

Table 4. Top differentially expressed pathways and processes in T2 MDSC compared to T2 granulocytes according to GO analysis. Gene ratio represents the number of regulated genes divided by the total number of pathway-related genes.

Of note, pathways involved in neutrophil activation and -function or T cell signaling and -activation also exhibited a high number of differentially regulated genes as identified by GO analysis, further emphasizing the impact of MDSC on immune function (Table 5).

Gene Ontology ID	Description	GeneRatio	p-value	padj	regulated genes
GO:0042119	neutrophil activation	0.040234702	3.70E-10	5.84E-08	288
GO:0002446	neutrophil mediated immunity	0.040234702	4.98E-10	7.65E-08	288
GO:0002283	neutrophil activation involved in immune response	0.039396479	8.28E-10	1.24E-07	282
GO:0043312	neutrophil degranulation	0.039117072	1.08E-09	1.58E-07	280
GO:0050852	T cell receptor signaling pathway	0.012992456	2.34E-07	1.88E-05	93
GO:0042110	T cell activation	0.033528919	1.45E-06	8.46E-05	240

Table 5. Differentially regulated pathways in T2 MDSC compared to T2 granulocytes imvovled in neutrophil activation and -function or T cell signaling and -activation according to GO. Gene ratio represents the number of regulated genes divided by the total number of pathway-related genes.

3.7 Comparison of T2 MDSC and T2 granulocytes - focus on T cell immunosuppressive genes

In order to identify additional genes and pathways that, besides L-Arginine breakdown, account for the immunosuppressive characteristics of MDSC, NGS data from T2 granulocytes and T2 MDSC were analyzed in a more detailed manner to identify genes that are highly expressed in T2 MDSC, show differential expression in T2 MDSC compared to T2 granulocytes and are known to impair T cell function. This revealed that a disproportionate number of genes (depicted in Table 6) involved in ROS formation or -inactivation display a differential expression in T2 granulocytes and T2 MDSC.

Gene ID	Protein Name	Function	log2foldchange	p-Value	padj
CYBA	cytochrome b-245 alpha chain	essential membrane-bound subunit of NADPH oxidase	0.25	0.011541	0.022334
CYBB (NOX2)	cytochrome b-245 beta chain	essential membrane-bound subunit of NADPH oxidase	-2.46	5.57E-38	1.25E-35
NCF1	p47phox	cytosolic subunit of neutrophil NADPH oxidase	0.76	8.83E-04	2.10E-03
NCF2	p67phox	cytosolic subunit of neutrophil NADPH oxidase	1	1.44E-17	2.11E-16
NCF4	p40phox	cytosolic regulatory component of neutrophil NADPH-oxidase	0.75	6.12E-07	2.35E-06
NOXA1	p51NOX	Activator of NOX1 and NOX2	-2.74	4.99E-08	2.21E-07
RAC1	Ras-related C3 botulinum toxin substrate 1	G-Protein, essential component of NADPH Oxidase	0.9	9.40E-33	1.02E-03

Table 6. Genes differentially expressed in T2 granulocytes and T2 MDSC with an impact on ROS formation or –inactivation.

Importantly, critical components or co-activators of the membrane-bound NADPH-Oxidase enzyme, namely NOXA1 and NOX2, were strongly induced in T2 MDSC (Table 6). In myeloid cells, NADPH-Oxidase is one of the central enzymes that mediate formation of Reactive Oxygen Species (ROS). ROS, in turn, induce oxidative stress and strongly impair T cell function by inducing protein modification, apoptosis and cellular damage.[40] Subsequent interaction analysis further underlines the importance of ROS-formation and -signaling in the context of MDSC-mediated immunosuppression after CPB as in-silico analysis using the STRING database revealed that all genes mentioned in Table 6 share a functional relationship, directly interact with each other and thus create a regulatory network (Fig. 17).

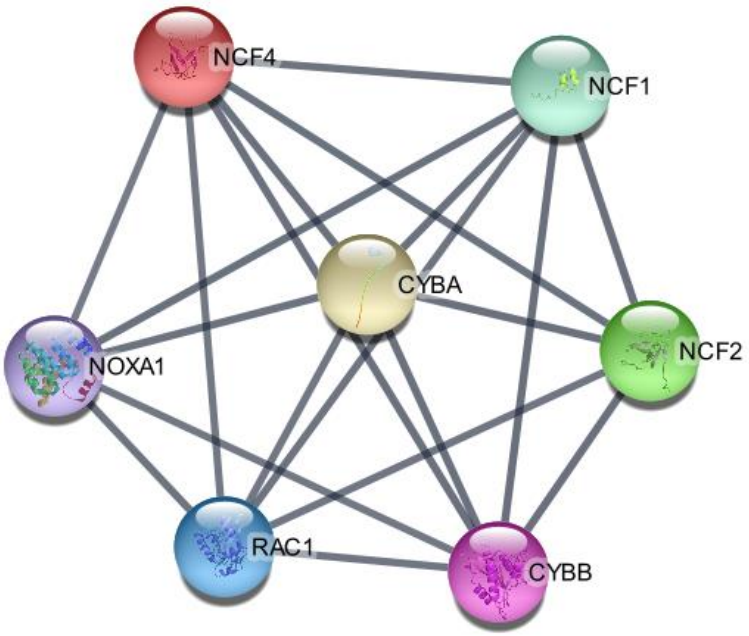

Figure 17. Regulatory network of differentially expressed genes involved in ROS-formation and –signalling. The interaction analysis databases STRING (string-db.org) and Cytoscape (cytoscape.org) were used to depict the interaction network. Interaction parameters were adjusted to no additional interaction partners and a prediction probability score cutoff of 0.91.

To further validate the strong MDSC-specific induction of enzymes involved in ROS-formation, gene expression of T2 PBMC, T2 PBMC that were depleted from MDSC by CD15 microbead separation and T2 MDSC was analyzed by qRT-PCR. This revealed that, compared to T2 PBMC, the MDSC fraction expressed unequivocally higher levels of CYBB (NOX2), the central component of the NADPH Oxidase (Fig. 18A, induction 3.18-fold ±0.2, n=10, $p<0.001$), whereas expression levels of the ROS-inactivating enzyme Superoxide Dismutase1 (SOD1) was significantly decreased (Fig. 18B, -62.2% ±7.6, n=10, $p<0.001$). Moreover, NGS analysis, validated by subsequent qRT-PCR, also revealed a dramatic induction of Myeloperoxidase (MPO), one of the best-studied enzymes involved in ROS formation, in T2 MDSC compared to T2 PBMC (Table 7 and Fig. 19, induction 171-fold ± 84, n=5, $p<0.001$).

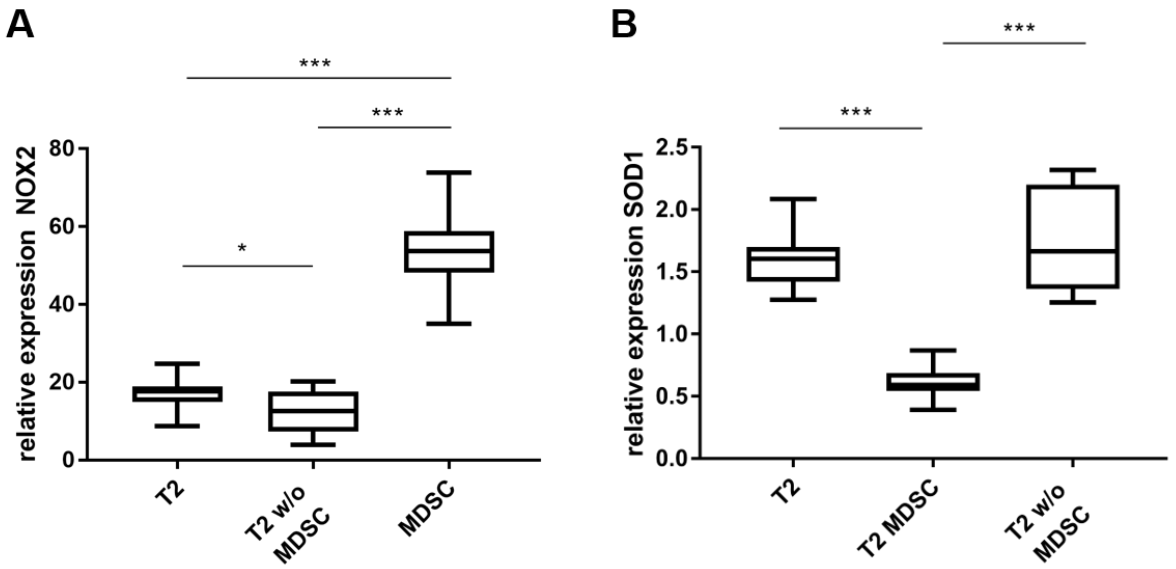

Figure 18. Expression of genes involved in ROS formation (MPO) and –inactivtion (SOD1) in T2 PBMC and T2 MDSC. A) qRT-PCR of NOX (n=10). B) qRT-PCR of SOD1 (n=6). Quantification was performed in T2 PBMC, T2 PBMC after MDSC depletion and T2 MDSC. MDSC were depleted using CD15 microbeads (p<=0.001 each).

Gene ID	Protein Name	Function	log2foldchange	p-Value	padj
MPO	Myeloperoxidase	ROS production	-8.055756165	1.22E-55	2.78E-52

Table 7. MPO expression in T2 MDSC compared to T2 granulocytes as measured by NGS.

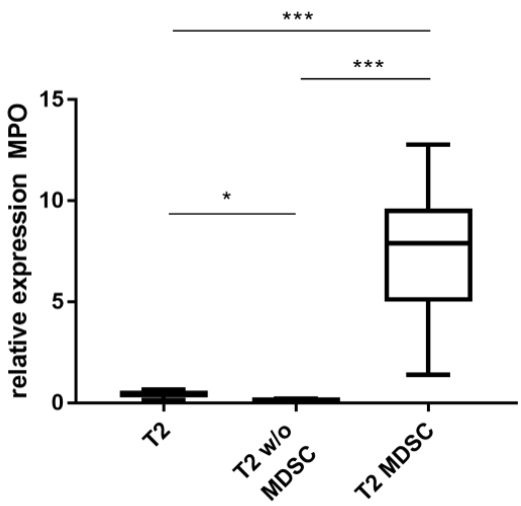

Figure 19. qRT-PCR of NOX (n=6, p<0.005). Quantification was performed in T2 PBMC, T2 PBMC after MDSC depletion and T2 MDSC. MDSC were depleted using CD15 microbeads.

Interestingly, STRING network analysis failed to directly link MPO with the NADPH-Oxidase network (Fig. 16), but identified MPO as a central node of a second network with all its interaction partners a) induced in MDSC and b) either involved in ROS formation or regulation of immune function (Fig. 20 and Table 8). Surprisingly, the same STRING analysis identified

ARG1, the MDSC-specific, L-Arginine-depleting, T cell immunosuppressive enzyme as a second central network hub besides MPO, interacting with all other network members. These results point towards a close relationship between L-Arginine metabolism and ROS formation in MDSC.

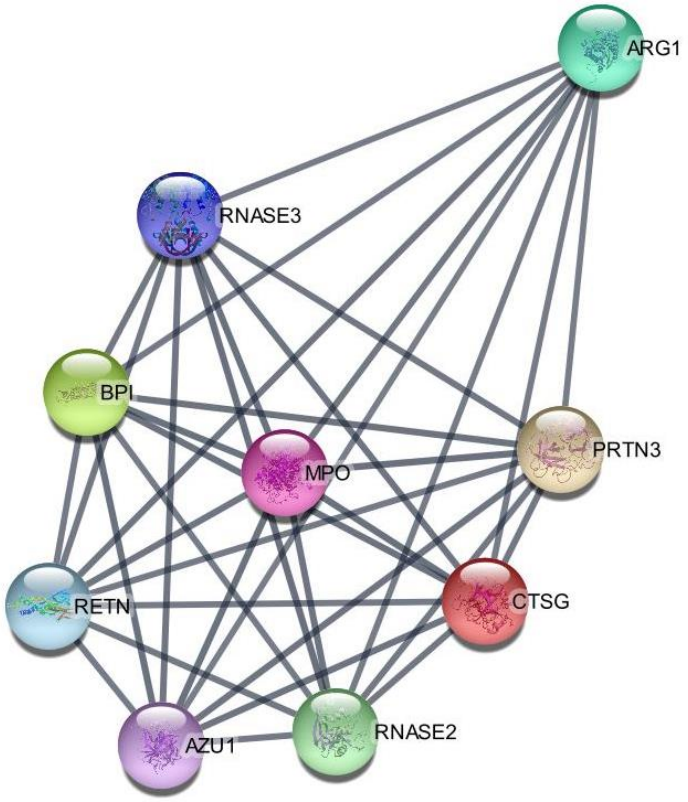

Figure 20. STRING analysis of putative interaction partners of MPO. STRING parameters were adjusted to one direct interaction partner of MPO with a prediction probability score cutoff of 0.91.

Gene ID	Protein Name	Function	log2foldchange	p-Value	padj
AZU1	Azurocidin 1	Antimicrobial peptide	-6.456306048	1.51E-42	5.94E-04
RNASE3	Eosinophil cationic protein	Antimicrobial peptide	-5.119529194	3.21E-26	1.42E-24
RNASE2	Eosinophil-Derived Neurotoxin	Antiviral, cytotoxic	-5.062334163	6.30E-35	9.54E-33
BP1	Bactericidal Permeability-Increasing Protein	antibiotic peptide, LPS binding	-2.705219336	2.11E-21	5.10E-20
RETN	Resistin	Proinflammatory cytokine	-5.161163094	2.10E-37	4.19E-35
CTSG	Cathepsin G	Protease, antibacterial	-7.651423506	1.29E-45	7.69E-43
PRTN3	Proteinase3	Proteolysis	-8.722043125	1.79E-34	2.51E-32

Table 8. Genes predicted to directly interact with MPO according to STRING analysis (Fig. 17) and their expression levels in T2 MDSC compared to T2 granulocytes according to NGS data.

3.8 ROS-Scavenging improves T cell function

So far, our experiments suggested that increased release of ROS by T2 MDSC might contribute to impaired T cell immunocompetence after CPB. In order to detect whether T cells after CPB are indeed exposed to higher ROS levels, we analyzed the intracellular concentration of reduced Glutathione (GSH). Glutathione, the most prevalent antioxidant in humans, is composed of the three amino acids Glutamate, Cysteine and Glycine. The reduced form of Glutathione, GSH, gets quickly oxidized by ROS and converts from a monomer into a dimer (Glutathione disulfide, GSSG), efficiently neutralizing ROS thus reducing the cell's oxidative stress level.[41] In a steady state, GSH is quickly replenished ATP-dependently. During CPB, however, we detected significantly reduced levels of intracellular GSH in lymphocytes on the first postoperative day (T3) (Fig. 21; -20.8% ±8.5, n=17, p=0.005), pointing towards higher oxidative stress levels after CPB and insufficient synthesis of GSH.[42]

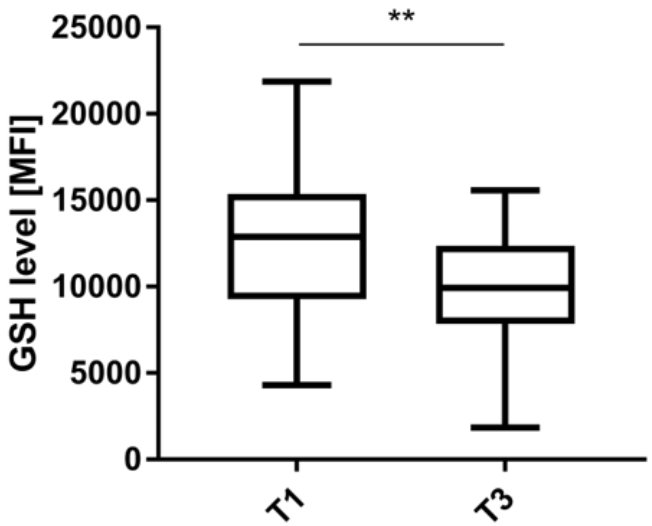

Figure 21. Intracellular levels of reduced Glutathione (GSH) in lymphocytes are reduced on the first postoperative day. GSH levels were measured using the ThiolTracker™ Violet Glutathione detection reagent by flow cytometry after gating for lymphocytes and doublet exclusion. T1: before CPB; T3: first postoperative day.

Next, we hypothesized that attenuation of this MDSC-triggered oxidative stress, possibly by replenishing GSH levels, might enhance T cell effector functions. For experimental proof, we incubated T2 PBMC in RPMI supplemented with either 5mM GSH or 5mM of the GSH precursor N-Acetyl-Cysteine (NAC) and indeed detected a clear improvement of T cell specific proliferation and IFNɣ secretion compared to controls (Fig. 22; proliferation: NAC +18% ±13.3; GSH: +26% ±10.6, both n=13, p=0.003; IFNɣ secretion: NAC: +45.8% ±26.9, n=5, p=0.005; GSH: +75.8%% ± 29.3, n= 5, p=0.041). These results suggest that ROS

scavenging by supplementation of NAC or GSH ameliorates the suppressive effect of MDSC on T cells and augment effector functions.

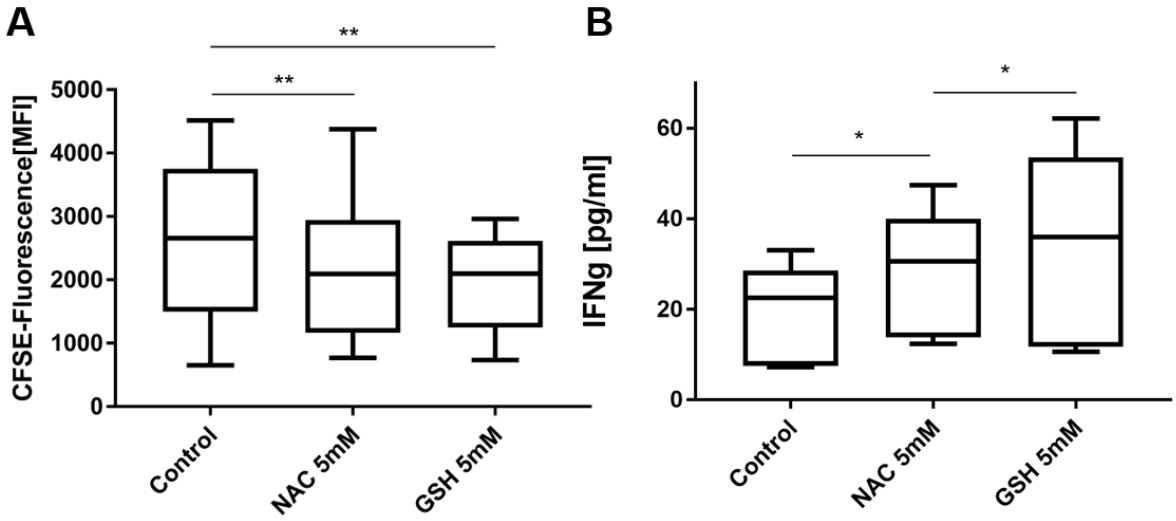

Figure 22. ROS scavenging by supplementation of GSH and NAC improves T cell effector functions. T2 PBMC were incubated in RPMI and supplemented with 5mM NAC or 5mM GSH, stimulated with anti CD3/CD28 microbeads and incubated for 5 days. PBMC without supplementation served as control. **A)** T cell proliferation rates as measured by CFSE dilution using flow cytometry after doublet exclusion. B) IFNγ levels in cell culture supernatant as quantified by ELISA. (n=7; *p<0.05; **p<0.01).

4. Discussion

The per se salutary procedure of CPB, indispensable in state-of-the-art cardiothoracic surgery, provokes several severe immunological side effects.[43–45] The initial hyperinflammatory phase after CPB is routinely controllable by anti-inflammatory treatment strategies and administration of catecholamines and declines within days.[44,46–48]

The concomitant long-lasting immunosuppressive state, however, frequently leads to postoperative complications such as wound healing disorders or secondary infections.[7,8,49,50] Approximately 5 - 8% of patients undergoing cardiac surgery develop a hospital-acquired infection (HAI), significantly increasing mortality and causing incremental healthcare costs of $ 20,000 - $ 40,000 per patient.[10,11,50]

Already 30 years ago, researchers observed severe dysfunctions of the immune system after CPB.[51,52] However, these studies focused on the description of impaired T cell cytokine secretion and did not investigate the underlying molecular mechanisms. So far, no therapeutic strategy exists that is able to dampen or even abrogate postoperative immunosuppression. Recently, we discovered that anergy of the adaptive immune system strongly contributes to post-CPB immunoparalysis and identified new aspects of its origin: CPB induces a transient accumulation of MDSC that strongly hampers T cell immunocompetence.[12]

Earlier studies detected MDSC during chronic inflammatory disorders including, but not limited to cancers[26,53–55] or autoimmune diseases[21,22,56] and identified them to substantially impair effector functions of adaptive immune cells.[18] MDSC presumably represent immature cells of the myeloid lineage and are not detected in healthy individuals except in neonates and during pregnancy.[17,57] Earlier studies, however, only provided scarce data regarding the molecular mechanisms that account for this potent immunosuppression. The fact that MDSC normally occur in an unpredictable time course and very low cell numbers made it difficult to establish a model that reliably and reproducibly triggers MDSC accumulation. However, we recently discovered that CPB induces a transient accumulation of considerable MDSC numbers in a reproducible manner.[12] This, for the first time, provides the opportunity to investigate MDSC in more detail.

In this thesis, we identified MDSC-specific mechanisms that contribute to T cell immunoparalysis after CPB: increased breakdown of L-Arginine and excessive production of ROS consecutively hamper T cell effector functions. Moreover, the first comprehensive NGS analysis of post-CPB MDSC and mature myeloid cell populations obtained after CPB was

performed to gain further insights into MDSC-specific molecular mechanisms that may account for their immunosuppressive potential.

L-Arginine is a conditionally (semi-)essential amino acid important for protein synthesis. In homeostatic conditions it can be synthesized in sufficient amounts by the Urea Cycle. During inflammatory conditions like SIRS, however, L-Arginine becomes an essential amino acid: amplified transcriptional activity and enhanced production of nitric oxide leads to a dramatic increase in L-Arginine demand significantly exceeding endogenous synthesis.[58,59] Importantly, recent data provided evidence that, besides its central role for protein synthesis, L-Arginine is indispensable for optimal T cell function: elevation of L-Arginine levels enhanced T cell survival, proliferation and anti-tumor activity in a mouse model.[60] In contrast, decrease of L-Arginine concentrations leads to reduced expression of the CD3 zeta chain (CD3ζ), an essential component of the T cell receptor, thus hampering T cell activation and eventually inhibiting T cell effector functions.[31,33] In the context of CPB, CD3ζ expression and T cell functions were also found to be strongly reduced on the first postoperative day.[12] In line with these results, our experimental data proved that L-Arginine serum levels were significantly decreased on the first postoperative day. *In-vitro* supplementation of L-Arginine, however, improved viability, proliferation and effector functions of T cells obtained after CPB, providing evidence for a causal relationship between L-Arginine levels and postoperative T cell dysfunction after cardiac surgery with the use of CPB.

Previous studies identified MDSC-mediated modulation of L-Arginine levels as a central mechanism of immunosuppression in chronic inflammatory conditions like autoimmune disorders or cancer.[53–55,61] This thesis, however, is the first describing increased breakdown of L-Arginine in an acute inflammatory setting. The results clearly show that MDSC rapidly accumulating after CPB specifically express high amounts of functional Arginase1, decrease L-Arginine serum levels and thus account for the T cell immunoparalysis observed after CPB.

However, studies suggest that L-Arginine breakdown is only one among several immunosuppressive mechanisms of MDSC[17] but -due to unpredictable occurrence and rather low MDSC numbers in chronic inflammatory disorders- data regarding gene expression and molecular mechanisms of MDSC are currently scarce.

Moreover, there is still much debate regarding the origin of MDSC: studies investigating samples from cancer patients suggested that MDSC resemble degranulated granulocytes that -due to a reduced density after degranulation- co-purify with PBMC in the buffy coat after Ficoll density gradient centrifugation and are termed LDG (Low-Density

granulocytes).[26] In contrast, other studies provide evidence that MDSC rather resemble immature cells of the myeloid lineage.[57,62] These studies, however, investigated MDSC during chronic inflammatory diseases, where MDSC accumulate in low amounts over a long period of time. Thus, in order to verify the validity of our experimental model, to gather information about the specific gene expression profiles of acutely occurring MDSC and to draw conclusions about their potential origin, we first compared gene expression profiles of mature granulocytes, LDG and MDSC by NGS analysis. This revealed high similarities between mature granulocytes and LDG indicating that these cell populations share a common origin. In contrast, comparison of NGS data of LDG and post-CPB MDSC revealed remarkable differences in gene expression. Notably, pathways important for gene and protein expression such as "RNA processing", "ribosome biogenesis" or "protein translation" were strongly induced in post-CPB MDSC, pointing towards a higher transcriptional and translational activity. These results stand in strong contrast to the aforementioned studies suggesting that MDSC simply represent LDG. Much more, our NGS data rather revealed a remarkable similarity between LDG and mature granulocytes.

However, these results did not prove that post-CPB granulocytes and -MDSC indeed significantly differ from each other. Thus, to ultimately provide proof and to further emphasize the translational relevance of our NGS analyses, we eventually compared post-CPB granulocytes and -MDSC. Again, this revealed a differential expression of approximately 14,000 genes. Interestingly, a disproportionate number of genes upregulated in MDSC regulate RNA trafficking or protein translation, corroborating the results from our LDG/MDSC comparison and again pointing towards a higher transcriptional activity of MDSC. These results ultimately corroborated that T2 MDSC -indeed- represent an individual cell entity with a unique gene expression profile that needs to be distinguished from mature granulocytes and their degranulated subpopulations.

More detailed analysis of the NGS dataset and subsequent qRT-PCR revealed a strong MDSC-specific expression of genes involved in ROS metabolism: In-silico analysis of the NGS dataset expression levels of the ROS-inactivating enzyme SOD1 were decreased, whereas large quantities of the ROS-generating enzymes NOX2 and MPO were detected in MDSC. Since excessive ROS formation hampers T cell immunocompetence, it appeared likely that this mechanism contributes to MDSC-mediated T cell dysfunction after CPB. Consequently, we assumed that reduction of ROS levels could help to restore T cell immunocompetence. Indeed, our in vitro experiments clearly corroborated this assumption:

supplementation of the ROS scavengers GSH and NAC resulted in a marked improvement of T cell effector functions, that is proliferation and IFNɣ cytokine secretion.

Taken together, this thesis identified two central mechanisms of MDSC-specific acute T cell immunosuppression: the reduction of L-Arginine availability and the increase of ROS formation. Moreover, *in-silico* network analysis discovered a direct interaction between ARG1 and the ROS-producing MPO network, pointing towards a redundant organization of immunosuppressive mechanisms in MDSC. To address this, we evaluated in-vitro supplementation strategies for both L-Arginine depletion and ROS formation to dampen their impact on T cell immunosuppression to pave the way for translational studies.

For L-Arginine, feasibility studies in healthy subject and even patients undergoing cardiac surgery proved that oral supplementation of L-Arginine and its precursor molecule L-Citrulline significantly increases L-Arginine serum levels in healthy subjects and produces no unwanted side effects ([63,64] and own unpublished data). In a cohort of 8 patients suffering from septic shock, intravenous infusion of L-Arginine decreased protein catabolism, and increased both serum L-Arginine levels and NO production without impairing hemodynamic stability.[65] Moreover, supplementation of GSH or NAC was successfully performed previously: clinical studies proved that oral or intravenous administration of GSH is safe, efficiently mitigates the progress of early Alzheimer's disease[66,67] and, in a second study, improves arterial circulation in patients suffering from peripheral obstructive arterial disease,[68,69] possibly via increasing bioavailability of nitric oxide.[70] NAC, however, is routinely used in the clinic orally and intravenously as an expectorant or as antidote for acetaminophen poisoning. As NAC and GSH were both already evaluated in clinical studies or routine use, both represent safe drugs that do not provoke significant adverse effects.

Collectively, this study is the first that provides a comprehensive NGS analysis of acute MDSC, comparing them with cells of the myeloid lineage. Our results clearly revealed that post-CPB MDSC exhibit a specific gene expression profile and thus need to be viewed as a unique cell population with specific properties. Moreover, we evaluated therapeutic strategies to abrogate MDSC-specific immunosuppression after CPB *in-vitro*. Here, however, clinical studies are needed to further clarify whether supplementation of L-Arginine, GSH and NAC might represent a safe yet powerful way to counteract or even prevent T cell dysfunction, reduce postoperative immunosuppression-associated complications and thus decrease healthcare costs and mortality in this particular patient cohort. This might gain importance not only during CPB but also in other MDSC-inducing pathologies.

5. References

1. Stoney, W. S. Evolution of cardiopulmonary bypass. *Circulation* **119**, 2844–2853 (2009).
2. Gaudino, M. *et al.* Off-pump coronary artery bypass grafting: 30 years of debate. *J. Am. Heart Assoc.* **7**, e009934 (2018).
3. Machin, D. & Allsager, C. Principles of cardiopulmonary bypass. *Contin Educ Anaesth Crit Care Pain* **6**, 176–181 (2006).
4. Xiao, W. *et al.* A genomic storm in critically injured humans. *J. Exp. Med.* **208**, 2581–2590 (2011).
5. Hall, M. W., Greathouse, K. C., Thakkar, R. K., Sribnick, E. A. & Muszynski, J. A. Immunoparalysis in Pediatric Critical Care. *Pediatr. Clin. North Am.* **64**, 1089–1102 (2017).
6. Hotchkiss, R. S., Monneret, G. & Payen, D. Immunosuppression in sepsis: a novel understanding of the disorder and a new therapeutic approach. *Lancet Infect. Dis.* **13**, 260–268 (2013).
7. Rankin, J. S. *et al.* Management of immune dysfunction after adult cardiac surgery. *J. Thorac. Cardiovasc. Surg.* **142**, 575–580 (2011).
8. Cornell, T. T. *et al.* Clinical implications and molecular mechanisms of immunoparalysis after cardiopulmonary bypass. *J. Thorac. Cardiovasc. Surg.* **143**, 1160–1166.e1 (2012).
9. Boomer, J. S. *et al.* Immunosuppression in patients who die of sepsis and multiple organ failure. *JAMA* **306**, 2594–2605 (2011).
10. Hadaya, J. *et al.* Impact of Postoperative Infections on Readmission and Resource Use in Elective Cardiac Surgery. *Ann. Thorac. Surg.* (2021) doi:10.1016/j.athoracsur.2021.04.013.
11. Greco, G. *et al.* Costs associated with health care-associated infections in cardiac surgery. *J. Am. Coll. Cardiol.* **65**, 15–23 (2015).
12. Hübner, M. *et al.* Myeloid-Derived Suppressor Cells Mediate Immunosuppression After Cardiopulmonary Bypass. *Crit. Care Med.* **47**, e700–e709 (2019).
13. Bronte, V. *et al.* Recommendations for myeloid-derived suppressor cell nomenclature and characterization standards. *Nat. Commun.* **7**, 12150 (2016).
14. Mielcarek, M., Martin, P. J. & Torok-Storb, B. Suppression of alloantigen-induced T-cell proliferation by CD14+ cells derived from granulocyte colony-stimulating factor-mobilized peripheral blood mononuclear cells. *Blood* **89**, 1629–1634 (1997).
15. Pak, A. S. *et al.* Mechanisms of immune suppression in patients with head and neck cancer: presence of CD34(+) cells which suppress immune functions within cancers that secrete granulocyte-macrophage colony-stimulating factor. *Clin. Cancer Res.* **1**, 95–103 (1995).
16. Lang, S. *et al.* Clinical Relevance and Suppressive Capacity of Human Myeloid-Derived Suppressor Cell Subsets. *Clin. Cancer Res.* **24**, 4834–4844 (2018).
17. Gabrilovich, D. I. Myeloid-Derived Suppressor Cells. *Cancer Immunol Res* **5**, 3–8 (2017).
18. Veglia, F., Sanseviero, E. & Gabrilovich, D. I. Myeloid-derived suppressor cells in the

era of increasing myeloid cell diversity. *Nat. Rev. Immunol.* (2021) doi:10.1038/s41577-020-00490-y.
19. Consonni, F. M. *et al.* Myeloid-Derived Suppressor Cells: Ductile Targets in Disease. *Front. Immunol.* **10**, 949 (2019).
20. Gielen, P. R. *et al.* Elevated levels of polymorphonuclear myeloid-derived suppressor cells in patients with glioblastoma highly express S100A8/9 and arginase and suppress T cell function. *Neuro. Oncol.* **18**, 1253–1264 (2016).
21. Wu, H. *et al.* Arginase-1-dependent promotion of TH17 differentiation and disease progression by MDSCs in systemic lupus erythematosus. *Sci. Transl. Med.* **8**, 331ra40 (2016).
22. Pang, B. *et al.* Myeloid-derived suppressor cells shift Th17/Treg ratio and promote systemic lupus erythematosus progression through arginase-1/miR-322-5p/TGF-β pathway. *Clin. Sci.* **134**, 2209–2222 (2020).
23. Yan, L. *et al.* The Immunoregulatory Role of Myeloid-Derived Suppressor Cells in the Pathogenesis of Rheumatoid Arthritis. *Front. Immunol.* **11**, 568362 (2020).
24. Guo, C. *et al.* Myeloid-derived suppressor cells have a proinflammatory role in the pathogenesis of autoimmune arthritis. *Ann. Rheum. Dis.* **75**, 278–285 (2016).
25. Baumann, T. *et al.* Regulatory myeloid cells paralyze T cells through cell-cell transfer of the metabolite methylglyoxal. *Nat. Immunol.* **21**, 555–566 (2020).
26. Rodriguez, P. C. *et al.* Arginase I–Producing Myeloid-Derived Suppressor Cells in Renal Cell Carcinoma Are a Subpopulation of Activated Granulocytes. *Cancer Res.* **69**, 1553–1560 (2009).
27. Marvel, D. & Gabrilovich, D. I. Myeloid-derived suppressor cells in the tumor microenvironment: expect the unexpected. *J. Clin. Invest.* **125**, 3356–3364 (2015).
28. Schwedhelm, E. *et al.* High-throughput liquid chromatographic-tandem mass spectrometric determination of L-Arginine and dimethylated L-Arginine derivatives in human and mouse plasma. *J. Chromatogr. B Analyt. Technol. Biomed. Life Sci.* **851**, 211–219 (2007).
29. Mortazavi, A., Williams, B. A., McCue, K., Schaeffer, L. & Wold, B. Mapping and quantifying mammalian transcriptomes by RNA-Seq. *Nat. Methods* **5**, 621–628 (2008).
30. Szklarczyk, D. *et al.* STRING v11: protein–protein association networks with increased coverage, supporting functional discovery in genome-wide experimental datasets. *Nucleic Acids Res.* **47**, D607–D613 (2018).
31. Rodriguez, P. C. *et al.* Regulation of T cell receptor CD3zeta chain expression by L-Arginine. *J. Biol. Chem.* **277**, 21123–21129 (2002).
32. Rodriguez, P. C. *et al.* Arginase I production in the tumor microenvironment by mature myeloid cells inhibits T-cell receptor expression and antigen-specific T-cell responses. *Cancer Res.* **64**, 5839–5849 (2004).
33. Zabaleta, J. *et al.* Helicobacter pylori arginase inhibits T cell proliferation and reduces the expression of the TCR zeta-chain (CD3zeta). *J. Immunol.* **173**, 586–593 (2004).
34. Bettini, M. L. *et al.* Cutting Edge: CD3 ITAM Diversity Is Required for Optimal TCR Signaling and Thymocyte Development. *J. Immunol.* **199**, 1555–1560 (2017).
35. Markewitz, A. *et al.* An imbalance in T-helper cell subsets alters immune response after cardiac surgery. *Eur. J. Cardiothorac. Surg.* **10**, 61–67 (1996).

36. Franke, A. *et al.* Exogenous IL-12 and its effect on TH1/TH2 cell activity after cardiac surgery. *Shock* **32**, 366–373 (2009).
37. Franke, A. *et al.* Hyporesponsiveness of T cell subsets after cardiac surgery: a product of altered cell function or merely a result of absolute cell count changes in peripheral blood? *Eur. J. Cardiothorac. Surg.* **30**, 64–71 (2006).
38. Sanchez-Pino, M. D., Dean, M. J. & Ochoa, A. C. Myeloid-derived suppressor cells (MDSC): When good intentions go awry. *Cell. Immunol.* **362**, 104302 (2021).
39. Rahman, S. *et al.* Low-density granulocytes activate T cells and demonstrate a non-suppressive role in systemic lupus erythematosus. *Ann. Rheum. Dis.* **78**, 957–966 (2019).
40. Nagaraj, S. *et al.* Altered recognition of antigen is a mechanism of CD8+ T cell tolerance in cancer. *Nat. Med.* **13**, 828–835 (2007).
41. Muri, J. & Kopf, M. Redox regulation of immunometabolism. *Nat. Rev. Immunol.* **21**, 363–381 (2021).
42. Belikov, A. V., Schraven, B. & Simeoni, L. T cells and reactive oxygen species. *J. Biomed. Sci.* **22**, 85 (2015).
43. Taylor, K. M. SIRS—The Systemic Inflammatory Response Syndrome after cardiac operations. *The Annals of Thoracic Surgery* vol. 61 1607–1608 (1996).
44. Paparella, D., Yau, T. M. & Young, E. Cardiopulmonary bypass induced inflammation: pathophysiology and treatment. An update. *Eur. J. Cardiothorac. Surg.* **21**, 232–244 (2002).
45. Stoppelkamp, S. *et al.* Identification of Predictive Early Biomarkers for Sterile-SIRS after Cardiovascular Surgery. *PLoS One* **10**, e0135527 (2015).
46. Warltier, D. C., Laffey, J. G., Boylan, J. F. & Cheng, D. C. H. The systemic inflammatory response to cardiac surgery: implications for the anesthesiologist. *The Journal of the American Society of Anesthesiologists* **97**, 215–252 (2002).
47. Baehner, T. *et al.* [Cardiopulmonary bypass in cardiac surgery]. *Anaesthesist* **61**, 846–856 (2012).
48. Day, J. R. S. & Taylor, K. M. The systemic inflammatory response syndrome and cardiopulmonary bypass. *Int. J. Surg.* **3**, 129–140 (2005).
49. Rankin, J. S., Glower, D. D., Teichmann, T. L., Muhlbaier, L. H. & Stratton, C. W. Immunotherapy for refractory pulmonary infection after adult cardiac surgery: immune dysregulation syndrome. *J. Heart Valve Dis.* **14**, 783–791 (2005).
50. Gelijns, A. C. *et al.* Management practices and major infections after cardiac surgery. *J. Am. Coll. Cardiol.* **64**, 372–381 (2014).
51. Haeffner-Cavaillon, N. *et al.* Induction of interleukin-1 production in patients undergoing cardiopulmonary bypass. *J. Thorac. Cardiovasc. Surg.* **98**, 1100–1106 (1989).
52. Markewitz, A. *et al.* Successful restoration of cell-mediated immune response after cardiopulmonary bypass by immunomodulation. *J. Thorac. Cardiovasc. Surg.* **105**, 15–24 (1993).
53. Gabrilovich, D. I. & Nagaraj, S. Myeloid-derived suppressor cells as regulators of the immune system. *Nat. Rev. Immunol.* **9**, 162–174 (2009).
54. Najjar, Y. G. *et al.* Myeloid-Derived Suppressor Cell Subset Accumulation in Renal Cell

Carcinoma Parenchyma Is Associated with Intratumoral Expression of IL1β, IL8, CXCL5, and Mip-1α. *Clin. Cancer Res.* **23**, 2346–2355 (2017).
55. Ouzounova, M. *et al.* Monocytic and granulocytic myeloid derived suppressor cells differentially regulate spatiotemporal tumour plasticity during metastatic cascade. *Nat. Commun.* **8**, 14979 (2017).
56. Ji, J. *et al.* MDSCs: friend or foe in systemic lupus erythematosus. *Cell. Mol. Immunol.* **16**, 937–939 (2019).
57. Veglia, F., Perego, M. & Gabrilovich, D. Myeloid-derived suppressor cells coming of age. *Nat. Immunol.* **19**, 108–119 (2018).
58. Morris, S. M., Jr. L-Arginine: beyond protein. *Am. J. Clin. Nutr.* **83**, 508S–512S (2006).
59. Wijnands, K. A. P., Castermans, T. M. R., Hommen, M. P. J., Meesters, D. M. & Poeze, M. L-Arginine and citrulline and the immune response in sepsis. *Nutrients* **7**, 1426–1463 (2015).
60. Geiger, R. *et al.* L-Arginine Modulates T Cell Metabolism and Enhances Survival and Anti-tumor Activity. *Cell* **167**, 829–842.e13 (2016).
61. Lamano, J. B. *et al.* Glioblastoma-Derived IL6 Induces Immunosuppressive Peripheral Myeloid Cell PD-L1 and Promotes Tumor Growth. *Clin. Cancer Res.* **25**, 3643–3657 (2019).
62. Gao, X. *et al.* Immunotherapy Targeting Myeloid-Derived Suppressor Cells (MDSCs) in Tumor Microenvironment. *Frontiers in Immunology* vol. 11 (2021).
63. Schwedhelm, E. *et al.* Pharmacokinetic and pharmacodynamic properties of oral L-citrulline and L-Arginine: impact on nitric oxide metabolism. *Br. J. Clin. Pharmacol.* **65**, 51–59 (2008).
64. Tepaske, R. *et al.* Effect of preoperative oral immune-enhancing nutritional supplement on patients at high risk of infection after cardiac surgery: a randomised placebo-controlled trial. *Lancet* **358**, 696–701 (2001).
65. Luiking, Y. C., Poeze, M. & Deutz, N. E. L-Arginine infusion in patients with septic shock increases nitric oxide production without haemodynamic instability. *Clin. Sci.* **128**, 57–67 (2015).
66. Zampagni, M. *et al.* Novel S-acyl glutathione derivatives prevent amyloid oxidative stress and cholinergic dysfunction in Alzheimer disease models. *Free Radic. Biol. Med.* **52**, 1362–1371 (2012).
67. Mandal, P. K., Shukla, D., Tripathi, M. & Ersland, L. Cognitive Improvement with Glutathione Supplement in Alzheimer's Disease: A Way Forward. *J. Alzheimers. Dis.* **68**, 531–535 (2019).
68. Arosio, E., De Marchi, S., Zannoni, M., Prior, M. & Lechi, A. Effect of glutathione infusion on leg arterial circulation, cutaneous microcirculation, and pain-free walking distance in patients with peripheral obstructive arterial disease: a randomized, double-blind, placebo-controlled trial. *Mayo Clin. Proc.* **77**, 754–759 (2002).
69. Koutakis, P. *et al.* Oxidative stress and antioxidant treatment in patients with peripheral artery disease. *Physiol Rep* **6**, e13650 (2018).
70. Prasad, A., Andrews, N. P., Padder, F. A., Husain, M. & Quyyumi, A. A. Glutathione reverses endothelial dysfunction and improves nitric oxide bioavailability. *J. Am. Coll. Cardiol.* **34**, 507–514 (1999).

6. Acknowledgments

I would first like to thank my supervisor, Prof. Dr. Dr. Simone Kreth, for providing an excellent laboratory environment, the close supervision and guidance and the great support that made it possible to successfully complete this project.

I would also like to thank Prof. Dr. Bernhard Zwißler for the continous support I experienced during pursuing PhD thesis.

Moreover, I would like to thank all members if the Kreth group, past or current, that made our laboratory one of my favourite places; I would like thank Jessica Drexler, Gudrun Prangenberg and Gaby Gröger not just for excellent technical assistance but also for the continous social support in or outside of the lab, also inclding hte numerous extracurricular activities we conducted together. Thank you to my colleges Martin Müller, David Effinger and Simon Hirschberger, always listening and providing advice not just as work colleagues but also as friends.

Finally, my thanks go to Katrin, Valentina and the rest of my family always providing unconditional support and sharing me with the laboratory. You were the support that made it possible at all to complete this thesis.

7. Appendix

Publications arising from this work:

Major parts of this thesis have been published in the Journal *Critical Care Medicine*:

Hübner, M. *et al.* Myeloid-Derived Suppressor Cells Mediate Immunosuppression After Cardiopulmonary Bypass. *Crit. Care Med.* **47**, e700–e709 (2019).

Other publications:

1. Möhnle, P. *et al.* MicroRNA-665 is involved in the regulation of the expression of the cardioprotective cannabinoid receptor CB2 in patients with severe heart failure. *Biochem. Biophys. Res. Commun.* **451**, 516–521 (2014).
2. Möhnle, P. *et al.* MicroRNA-146a controls Th1-cell differentiation of human CD4+ T lymphocytes by targeting PRKCε. *Eur. J. Immunol.* **45**, 260–272 (2015).
3. Heyn, J. *et al.* miR-124a and miR-155 enhance differentiation of regulatory T cells in patients with neuropathic pain. *J. Neuroinflammation* **13**, 248 (2016).
4. Hinske, L. C. *et al.* Intronic miRNA-641 controls its host Gene's pathway PI3K/AKT and this relationship is dysfunctional in glioblastoma multiforme. *Biochem. Biophys. Res. Commun.* **489**, 477–483 (2017).
5. Schmieder, S. *et al.* Ultrasensitive SPR detection of miRNA-93 using antibody-enhanced and enzymatic signal amplification. *Eng. Life Sci.* **17**, 1264–1270 (2017).
6. Kreth, S., Hübner, M. & Hinske, L. C. MicroRNAs as Clinical Biomarkers and Therapeutic Tools in Perioperative Medicine. *Anesth. Analg.* **126**, 670–681 (2018).
7. Hübner, M., Galante, P. A. F., Kreth, S. & Hinske, L. C. Identification and Validation of Potential Differential miRNA Regulation via Alternative Polyadenylation. *Methods Mol. Biol.* **1733**, 87–92 (2018).
8. Möhnle, P. *et al.* MicroRNAs 143 and 150 in whole blood enable detection of T-cell immunoparalysis in sepsis. *Mol. Med.* **24**, 54 (2018).
9. Hübner, M. *et al.* Intronic miR-744 Inhibits Glioblastoma Migration by Functionally Antagonizing Its Host Gene MAP2K4. *Cancers* **10**, (2018).
10. Kammerer, T. *et al.* Changes of hemodynamic and cerebral oxygenation after exercise in normobaric and hypobaric hypoxia: associations with acute mountain sickness. *Ann Occup Environ Med* **30**, 66 (2018).

11. Heun, Y. *et al.* Inactivation of the tyrosine phosphatase SHP-2 drives vascular dysfunction in Sepsis. *EBioMedicine* (2019) doi:10.1016/j.ebiom.2019.03.034.
12. Hirschberger, S. *et al.* Identification of suitable controls for miRNA quantification in T-cells and whole blood cells in sepsis. *Sci. Rep.* **9**, 15735 (2019).
13. Kammerer, T. *et al.* Effects of balanced hydroxyethyl starch 6% (130/0.4) and albumin 5% on clot formation and glycocalyx shedding: Subgroup analysis of a prospective randomized trial. *Thromb. Res.* **183**, 111–118 (2019).
14. Hübner, M. *et al.* The IL-1 Antagonist Anakinra Attenuates Glioblastoma Aggressiveness by Dampening Tumor-Associated Inflammation. *Cancers* **12**, (2020).
15. Hübner, M. *et al.* MicroRNA-93 acts as an 'Anti-Inflammatory Tumor Suppressor' in Glioblastoma. *Neuro Oncol Adv* (2020) doi:10.1093/noajnl/vdaa047.
16. Tomasi, R. *et al.* T-Cell Response in a Cardiac Xenotransplant Model. *Exp. Clin. Transplant.*

LMU LUDWIG-MAXIMILIANS-UNIVERSITÄT MÜNCHEN

Dean's Office
Medical Faculty

MMRS MUNICH MEDICAL RESEARCH SCHOOL

Affidavit

Max Bernhard Hübner

Surname, first name

Guardinistr. 89

Street

81375 Munich

Zip code, town

Germany

Country

I hereby declare, that the submitted thesis entitled

MDSC-specific mechanisms of T cell immunosuppression after Cardiopulmonary Bypass

is my own work. I have only used the sources indicated and have not made unauthorised use of services of a third party. Where the work of others has been quoted or reproduced, the source is always given.

I further declare that the submitted thesis or parts thereof have not been presented as part of an examination degree to any other university.

Munich, June 15th, 2021

Place, date

Dr. med. Max Hübner

Signature doctoral candidate

LMU LUDWIG-MAXIMILIANS-UNIVERSITÄT MÜNCHEN

Dean's Office
Medical Faculty

MMRS MUNICH MEDICAL RESEARCH SCHOOL

Confirmation of Congruency between Printed and Electronic Version of the Doctoral Thesis

Hübner, Max Bernhard

Surname, first name

Guardinistr. 89

Street

81375

Zip code, town

Germany

Country

I hereby declare that the electronic version of the submitted thesis, entitled

MDSC-specific mechanisms of T cell immunoparalysis after Cardiopulmonary Bypass

is congruent with the printed version both in content and format.

Munich, June 15th, 2021

Place, date

Dr. med. Max Hübner

Signature doctoral candidate